Title
Planet Candidates from K2 Campaigns 5–8 and Follow-up Optical Spectroscopy

Authors
Petigura, Erik A
Crossfield, Ian JM
Isaacson, Howard
et al.

Peer reviewed

PLANET CANDIDATES FROM K2 CAMPAIGNS 5–8 AND FOLLOW-UP OPTICAL SPECTROSCOPY

Erik A. Petigura[1,9,10], Ian J. M. Crossfield[2,3], Howard Isaacson[4], Charles A. Beichman[5], Jessie L. Christiansen[5], Courtney D. Dressing[1,4], Benjamin J. Fulton[1,6,11,12], Andrew W. Howard[1], Molly R. Kosiarek[3,12], Sébastien Lépine[7], Joshua E. Schlieder[8], Evan Sinukoff[6,1], and Samuel W. Yee[1]

[1]California Institute of Technology, Pasadena, CA, 91125, USA

[2]Department of Physics, Massachusetts Institute of Technology, Cambridge, MA, USA

[3]University of California Santa Cruz, Santa Cruz, CA, 95064, USA

[4]Department of Astronomy, University of California, Berkeley, CA 94720, USA

[5]NASA Exoplanet Science Institute & Infrared Processing and Analysis Center, California Institute of Technology, Pasadena, CA, 91125, USA

[6]Institute for Astronomy, University of Hawai'i, Honolulu, HI 96822, USA

[7]Department of Physics & Astronomy, Georgia State University, Atlanta, GA, 30303, USA

[8]NASA Goddard Space Flight Center, 8800 Greenbelt Road, Greenbelt, MD 20771, USA

[9]petigura@caltech.edu

[10]Hubble Fellow

[11]Texaco Fellow

[12]NSF Graduate Research Fellow

ABSTRACT

We present 151 planet candidates orbiting 141 stars from *K2* campaigns 5–8 (C5–C8), identified through a systematic search of *K2* photometry. In addition, we identify 16 targets as likely eclipsing binaries, based on their light curve morphology. We obtained follow-up optical spectra of 105/141 candidate host stars and 8/16 eclipsing binaries to improve stellar properties and to identify spectroscopic binaries. Importantly, spectroscopy enables measurements of host star radii with ≈10% precision, compared to ≈40% precision when only broadband photometry is available. The improved stellar radii enable improved planet radii. Our curated catalog of planet candidates provides a starting point for future efforts to confirm and characterize *K2* discoveries.

Keywords: editorials, notices — miscellaneous — catalogs — surveys

1. INTRODUCTION

NASA's *Kepler Space Telescope*, operating in its prime mission (2009–2013; Borucki et al. 2010), shed light on many fundamental properties of exoplanets. Among these are the occurrence of planets as small as Earth around Sun-like and low-mass stars (e.g. Petigura et al. 2013; Dressing & Charbonneau 2015) and the diversity of planetary bulk compositions (Marcy et al. 2014; Weiss & Marcy 2014; Rogers 2015) extending down to Earth-size (e.g. Howard et al. 2013; Jontof-Hutter et al. 2015).

Now operating in its two-wheel *K2* mode (Howell et al. 2014), *Kepler* observes a different region of sky every three months. *K2* is conducting a wider, more shallow survey that complements the narrow, deep survey of the prime mission. Among its many accomplishments to date, *K2* has significantly increased the number of transiting planets around moderately bright stars (Crossfield et al. 2016), which will enable more detailed studies of exoplanet bulk composition using precision radial ve-

locity facilities. *K2* has also revealed planets around newborn stars (David et al. 2016; Mann et al. 2016) and planets around white-dwarfs (Vanderburg et al. 2015). Due to community-driven target selection, a large fraction of the *K2* targets are M-dwarfs, resulting in the detection of planets in or near the habitable zone (e.g. Crossfield et al. 2015; Montet et al. 2015; Petigura et al. 2015; Schlieder et al. 2016).

In this paper, we provide a catalog of planet candidates and eclipsing binaries from the second year of *K2* operations, corresponding to campaigns 5–8 (C5–C8). Section 2 presents our methodology for correcting spacecraft systematics in *K2* photometry and identifying planet candidates. In Section 3, we describe our spectroscopic follow-up program and present refined stellar parameters enabled by these spectra. We present our catalog of planet candidates and eclipsing binaries in Section 4 and summarize our findings in Section 5.

2. IDENTIFYING PLANET CANDIDATES

2.1. *Photometry*

During its prime mission, *Kepler* achieved photometric precisions of ≈ 40 ppm on 6.5 hour timescales (Christiansen et al. 2012) for targets of ≈ 12 mag in the *Kepler* bandpass (i.e. $Kp \approx 12$ mag). For many stars, photometric precision was limited by intrinsic stellar variability rather than photon-limited or instrumental errors. This exquisite precision was due in large part to stable pointing enabled by four (and later three) reaction wheels which stabilized the telescope against solar radiation pressure across the three axes of the telescope. Photometry for individual target stars was extracted using stationary software apertures composed of integer numbers of connected pixels.

During *K2* operations, where the spacecraft uses the two remaining operational reaction wheels, solar radiation pressure causes drifts of ~ 1 pixel to occur on ~ 6 hr timescales. As stars drift across the CCD, variations in pixel sensitivities and variable aperture losses result in apparent brightness variations.

Several techniques have been developed to correct for the position-dependent brightness variations due to the unstable platform of *K2*. A non-exhaustive list includes `k2sff` (Vanderburg & Johnson 2014), `k2phot` (Crossfield et al. 2015; Petigura et al. 2015; Crossfield et al. 2016), and `k2sc` (Aigrain et al. 2015) which model stellar brightness as a function of spacecraft orientation with a function and remove it from the light curve. The `everest` package (Luger et al. 2016) builds on the pixel-level decorrelation (PLD) approach developed for *Spitzer* (Deming et al. 2015) and decorrelates against the pixel-by-pixel photometric timeseries.

We generated light curves for 87913 stars observed by *K2* during C5–C8 using the publicly-available `k2phot` Python package.[1] The general methodology is described in previous works (Crossfield et al. 2015; Petigura et al. 2015; Crossfield et al. 2016). However, due to the evolving nature of *K2* systematics, we have continued to adapt and refine `k2phot` and summarize the methodology below.

Since systematics in the photometry are largely due to pointing drifts, accurate knowledge of the spacecraft orientation is important for removing orientation-dependent systematics. We characterize the time-dependent orientation of the *Kepler* spacecraft by analyzing the positions of ≈ 100 bright but unsaturated stars having $Kp \approx 12$ mag on a representative output channel of the *Kepler* CCD.[2] For each long-cadence integration,

we solve for the affine transformation that maps that frame to an arbitrary reference frame. We then use the sequence of affine transformations to transform a reference pixel coordinate on a reference frame[3] to the pixel coordinate on all other frames in the campaign.

We extract photometry using stationary apertures. Aperture size is described by a single variable N_{pix}, the number of pixels in the aperture. Apertures are constructed to accommodate image motion during a campaign. We construct apertures using a composite image constructed from the 90th percentile intensity value of all frames in a campaign. Because the stars move during *K2* observations, the 90th percentile image is smeared out and the apertures constructed from this image accommodate the drifts, mitigating severe aperture losses. The apertures are then constructed by selecting the pixel closest to the expected position of the target star, as predicted by the WCS coordinates provided by the *K2* project. Additional pixels are added iteratively by selecting the brightest pixel touching the current mask.

During the photometric extraction, we search for the aperture size $N_{\mathrm{pix,min}}$ that minimizes noise on three-hour times scales. This aperture size strikes a balance between the desire to minimize systematic noise which grows with *decreasing* aperture size, and background noise, which grows with *increasing* aperture size. We select an initial size $N_{\mathrm{pix,0}}$, which is motivated by previous analyses of stars with similar Kp. We then try six logarithmically-spaced N_{pix} between $N_{\mathrm{pix,0}}/4$ and $N_{\mathrm{pix,0}} \times 4$, which samples a curve describing noise as a function of N_{pix}. We find $N_{\mathrm{pix,min}}$ using upto three iterations of Newton's method. While testing different aperture sizes, we constrain N_{pix} to be between nine pixels and the total number of pixels in the target pixel file.

After extraction of the photometry we have a sequence of flux as a function of x, y, and t. We model out changes in flux that correlate with changes in x, y, and t using a Gaussian process with a squared-exponential covariance kernel, which is characterized by the following seven hyper-parameters A_x, l_x, A_y, l_y, A_t, l_t, and σ. Here, A corresponds to the amplitude of the GP, l corresponds to characteristic length scale, and σ accounts for a white noise component. Choosing the appropriate hyper-parameters can be computationally intensive on a star-by-star basis. We therefore adopt a scheme from Aigrain et al. (2015) which optimizes the hyper-parameters on a subset of the photometry using

---

[1] https://github.com/petigura/k2phot (commit a0d507)

[2] The *Kepler* CCD contains 84 output channels (Kepler Instru-

ment Handbook; Van Cleve et al. 2016), of which 76 were operational during C5-C8. An additional module (4 output channels) failed during C10.

[3] For example, a pixel on row 500, column 500, and frame 2000.

a differential evolution global optimizer (Storn & Price 1997).

We produced light curves for 87913 stars in C5–C8, which are available on the Exoplanet Follow-up Observing Program (ExoFOP) website.[4] Along with the photometry, we included photometric diagnostic plots showing the extraction aperture and resulting detrended light curve. Figure 1 shows these diagnostic plots for an example planet candidate around EPIC-211736671.

2.2. *Transiting Planet Search*

Our general transit search and vetting process is similar to that described in Crossfield et al. (2016). We give a brief summary of here. We searched the calibrated photometry for transiting planets using the publicly-available TERRA algorithm.[5] TERRA is a matched filter-based approach and is described by Petigura et al. (2013). TERRA convolves the photometry with a box-shaped approximation of a transit profile to compute a Single Event Statistic (SES) at every *K2* long-cadence measurement. The SES time series is phase-folded according to a finely-spaced grid of trial periods P and times of first transit T_0.

A classical matched-filter algorithm would then compute a Multiple Event Statistic (MES) by summing SES at each trial (P, T_0), which is optimal given uncorrelated Gaussian noise . However, in *K2* photometry we observe more frequent non-Gaussian anomalies relative to *Kepler* prime photometry due to the aggressive detrending that must be performed in order to remove the instrumental systematics described above. A traditional MES computation resulted in many spurious peaks with apparently high MES, but were later easily identifiable as anomalies through inspection. We address outliers by calculating MES only after removing the two highest SES peaks at each trial (P, T_0). Spurious peaks due to the chance alignment of two outliers are eliminated. This non-linear filter removes many spurious detections and eases the burden during manual vetting, described below. One consequence is that TERRA does not identify planets with one or two transits occurring in a *K2* campaign. Such transits are sometimes identified by eye, but we caution that many are likely overlooked. These events are especially amenable to searches by citizen scientists (see e.g., Christiansen et al. *accepted in AJ*).[6]

TERRA identifies ∼1000 Threshold-Crossing Events (TCEs) per campaign. A TCE is a particular combination of (P, T_0) that has MES that exceeds some threshold, but may not be an astrophysical transit. If a candidate has a periodic dimming of a consistent shape it is elevated to the status of a "*K2* Object of Interest" (K2OIs) which are consistent with an astrophysical transit or eclipse.

Our team visually inspects each K2OI to look for a robust indication that the target is an eclipsing binary. We look for secondary eclipses, which indicate that the transiting object is self-luminous and not a planet. Secondary eclipses associated with binaries with circular orbits are shifted in phase from the primary eclipse by 180°. We search for secondary eclipses at all phases to allow for eccentric orbits. We also look for obvious odd/even variations, which indicate that TERRA has identified a nearly circular EB at half the orbital period. We also identify stars that show variability that is phase-locked to the eclipse, which is a strong indicator of star-star modulation (ellipsoidal, reflection, or relativistic beaming).

Our eclipsing binary designation does not incorporate transit depth or whether the light curve is V-shaped. While these attributes are strong indicators of EB status, they are not conclusive. Planets transiting small M-dwarf stars can easily produce transits deeper than 1% and short period transits may appear V-shaped due to the 30-minute sampling of *K2*. We defer a detailed false positive calculation for a later paper.

In total, we identified 167 K2OIs, associated with 157 stars. Of these, 16/167 are likely eclipsing binaries, and we refer to the remaining 151 as planet candidates.

2.3. *Light Curve Fitting*

We fit the calibrated photometry according to the methodology of Crossfield et al. (2016). In brief, we used the publicly-available batman light curve code (Kreidberg 2015) to generate model light curves which we then compared against the photometry. We first derived a maximum likelihood solution and then derived parameter uncertainties using Markov Chain Monte Carlo (MCMC).[7]

In our modeling, the following parameters are allowed to vary: time of first transit T_0, orbital period P, inclination i, scaled semi-major axis $a/R_\star$, planet-star radius ratio $R_P/R_\star$, orbital eccentricity e, longitude of periastron ω, linear limb-darkening coefficient u, fractional light curve dilution δ, and the out-of-transit flux level.

During the fitting, we adopted the following priors:

- *Period.* Gaussian prior centered on maximum likelihood P having dispersion of 0.01 days.[8]

(a)

(b)
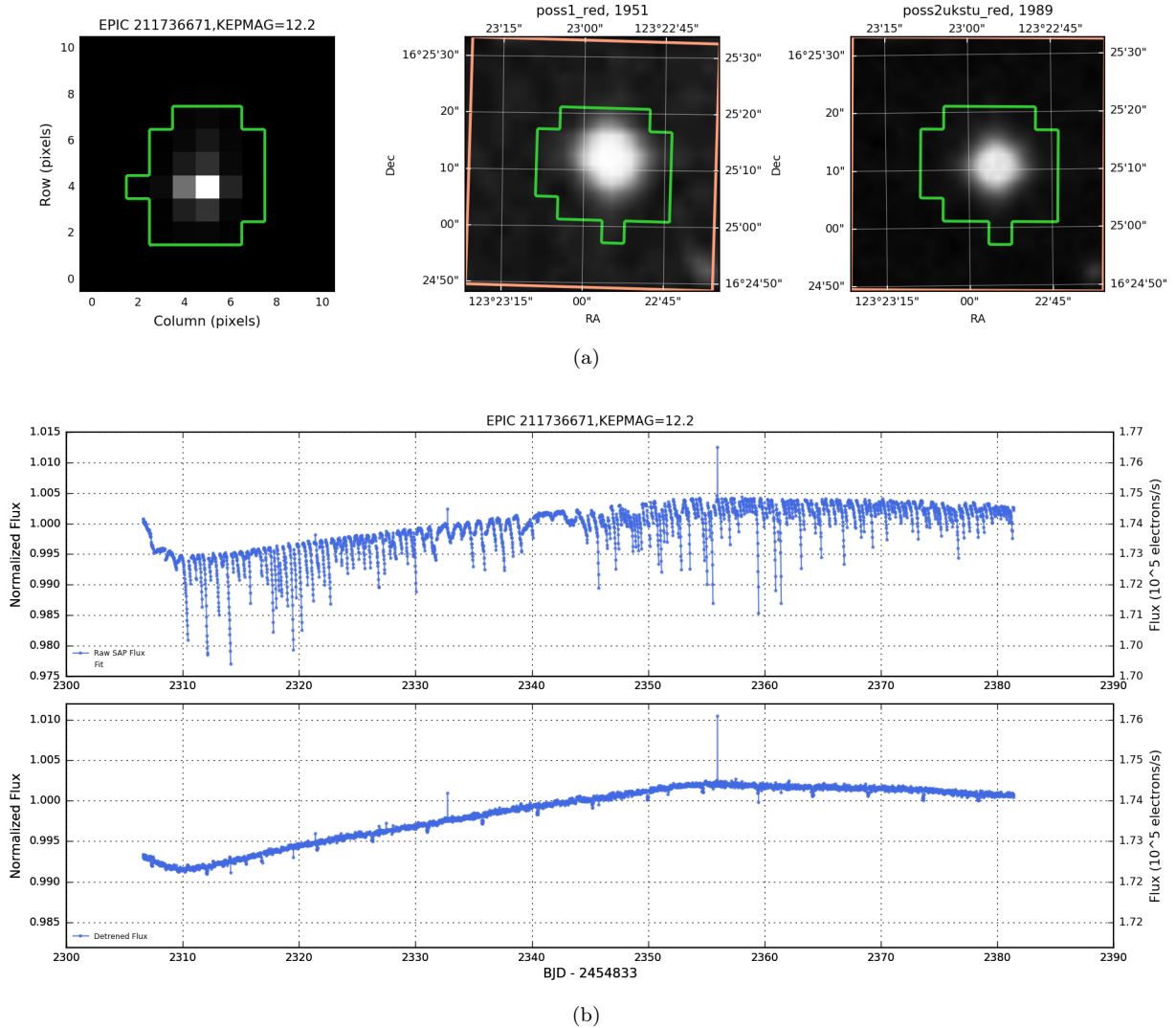
Figure 1. An example of the photometric diagnostic plots included as standard data products on the ExoFOP. Panel **(a)**: three images of an example planet candidate (EPIC-211736671), observed in C5. *Left:* the median of all long cadence C5 frames with the optimal extraction aperture shown in green. *Center:* the same region of sky as observed by the first Palomar Observatory Sky Survey (POSS-I). The orange region corresponds to the boundaries of the K2 frame. *Right:* the same region of sky as observed by POSS-II. Panel **(b):** aperture photometry before and after subtraction of our systematic noise model.

- *Time of transit.* Uniform prior centered on maximum likelihood T_0 having dispersion of $0.06 \times P$.

- *Radius ratio.* Uniform prior, $R_P/R_\star = [-1,+1]$. Following Eastman et al. (2013), we allow for negative $R_P/R_\star$ in our sampling to avoid the Lucy-Sweeney-type bias that results from treating $R_P/R_\star$ as a positive-definite quantity (Lucy &

Sweeney 1971).

- *Eccentricity.* Gaussian prior centered at 10^{-4} having dispersion of 10^{-3}. This effectively restricts the orbits to circular.

- *Longitude of periastron.* Uniform prior, $\omega = [0,2\pi]$.

- *Inclination.* Uniform prior, $i = [50°,90°]$.

- *Limb-darkening.* Gaussian prior on u where the mean and dispersion are computed using the publicly-available Limb-Darkening Toolkit (LDTK; Parviainen & Aigrain 2015). LDTK computes the distribution of u given Gaussian constraints on $T_{\rm eff}$, $\log g$, and [Fe/H]. For con-

walkers from jumping too far from the likelihood mode and wandering away. After performing the MCMC exploration, we verified that P and T_0 were more tightly constrained by the photometry than by the priors. The uncertainties on T_0 are typically 2.5% of the prior width (median value) and no more than 50% the prior width. The uncertainties on P are typically 2% of the prior width (median value) and no more than 60% the prior width.

sistency, we used $T_{\rm eff}$, $\log g$, and [Fe/H] constrained by broadband photometry from Huber et al. (2016). While photometrically-constrained $\log g$ and [Fe/H] are low-precision, u is only weakly dependent on these parameters, and the derived transit parameters are only weakly dependent on u.

- *Dilution.* Log-uniform prior, $\log \delta = [10^{-6}, 10^0]$. Our fits do not incorporate dilution constraints, so δ always reverts to the prior. We include δ so we can incorporate dilution constraints at later times.[9]

In Table 1, we report 1σ credible ranges on P, T_0, $R_P/R_\star$, transit duration T_{14}, and impact parameter b.

3. SPECTROSCOPY

3.1. *Spectroscopic Follow Program*

As a part of our team's standard follow-up efforts, we obtained optical spectra of 143 C5–C8 target stars using the HIgh Resolution Echelle Spectrometer (HIRES; Vogt et al. 1994) on the Keck-I 10 m telescope. We gathered spectra for the purpose of improving host star parameters and to place limits on the presence of companion stars with small separations through searches for spectroscopic binaries (SB2s). We aimed to obtain a spectrum of every K2OI brighter than $V = 14.0$ mag. For G stars, this limit corresponds roughly to $Kp = 13.6$ mag.

Table 2 lists the C5–C8 targets that we observed with HIRES, along with the results from our stellar characterization and search for spectroscopic binaries, which are described in Sections 3.2 and 3.3, respectively. We obtained HIRES spectra of 105/141 of the planet candidate host stars and for 8/16 of the likely EBs. In addition, we observed 30 other C5–C8 targets that we did not identify as candidates. These were typically observed because they were identified as planet candidates by other groups.

We used the HIRES exposure meter to obtain consistent SNR levels depending on V-band apparent magnitude: SNR = 45 ($V < 13.0$ mag), SNR = 32 ($V = 13.0 - 14.0$ mag), and SNR = 20 ($V > 14.0$ mag). Exposure times ranged from ≈ 10 s for $V = 9$ mag targets to ≈ 400 s for $V = 15$ mag targets. SNR is computed per reduced HIRES pixel on blaze at 5500 Å. Our HIRES follow-up was nearly complete down to $V = 14$ mag. Figure 2 shows the distribution of candidate hosts as a
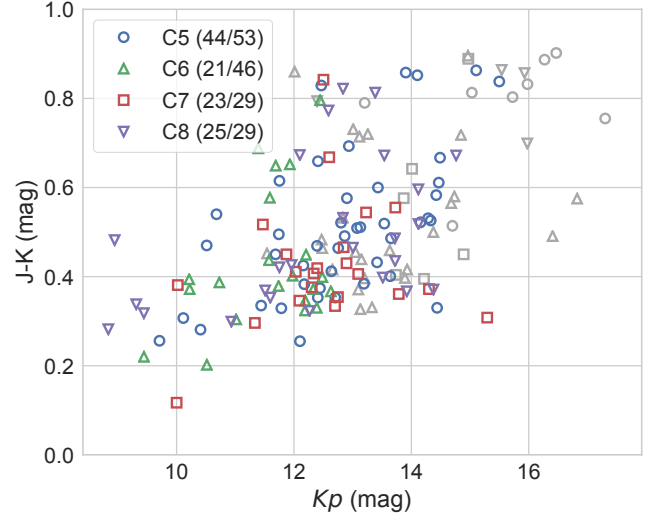
Figure 2. Distribution of K2OIs as a function of Kp and $J-K$ color. The colored/gray points represent targets with/without a HIRES spectrum. The marker color and shape represent a target's specific *K2* campaign. The HIRES follow-up is nearly complete to $Kp = 14$ mag.

function of Kp and $J-K$ color. The candidates with HIRES spectra are labeled. Figure 3 shows a spectral segment for one K2OI to illustrate typical spectral resolution and SNR level.

3.2. *Stellar Characterization*

We used our spectra to improve the precision of stellar and planetary properties such as $R_\star$ and R_P. We analyzed each spectrum with one of two related publicly-available codes: `SpecMatch-Syn` (Petigura 2015)[10] and `SpecMatch-Emp` (Yee et al. 2017).[11]

`SpecMatch-Syn` fits five regions of optical spectrum by interpolating within a grid of model spectra from Coelho et al. (2005). Recently, `SpecMatch-Syn` enabled a homogeneous analysis of 1305 spectra of planet hosts identified during the prime *Kepler* mission (Petigura et al. 2017). For stars with $T_{\rm eff} = 4700$–6500 K and $v\sin i < 20$ km s^{-1}, `SpecMatch-Syn` achieves precisions of 60 K in $T_{\rm eff}$, 0.10 dex in $\log g$, and 0.04 dex in [Fe/H], and 1 km s^{-1} in $v\sin i$.

We converted $T_{\rm eff}$, $\log g$, and [Fe/H] into $M_\star$ and $R_\star$ using the publicly-available `isoclassify` Python package (Huber et al. 2017),[12] which uses the MESA Isochrones and Stellar Tracks (MIST) database (Choi et al. 2016; Paxton et al. 2011, 2013, 2015). While `SpecMatch-Syn` returns $T_{\rm eff}$ precise to 60 K, as tested

---

[9] The non-zero prior on δ slightly alters the derived value of $R_P/R_\star$. However, because the median δ is 10^{-3}, this amounts to a fractional change in derived radius ratio of $\Delta(R_P/R_\star)/(R_P/R_\star) \approx \delta/2 = 5 \times 10^{-4}$, which may be ignored.

[10] https://github.com/petigura/specmatch-syn

[11] https://github.com/samuelyeewl/specmatch-emp

[12] https://github.com/danxhuber/isoclassify

Figure 3. Example HIRES characterization spectrum with `SpecMatch-Emp` fit. Blue spectrum is of EPIC212006344, an M0 dwarf, and illustrates the typical SNR from our characterization program of ≈ 45/pixel. The spectrum contains a dense forest of molecular lines, making *ab initio* spectral synthesis challenging. Red spectra are drawn from `SpecMatch-Emp` library and are identified as similar to the target spectrum by the `SpecMatch-Emp` algorithm. The green and black spectra are the best-fitting linear combination spectrum and residual spectrum, respectively.
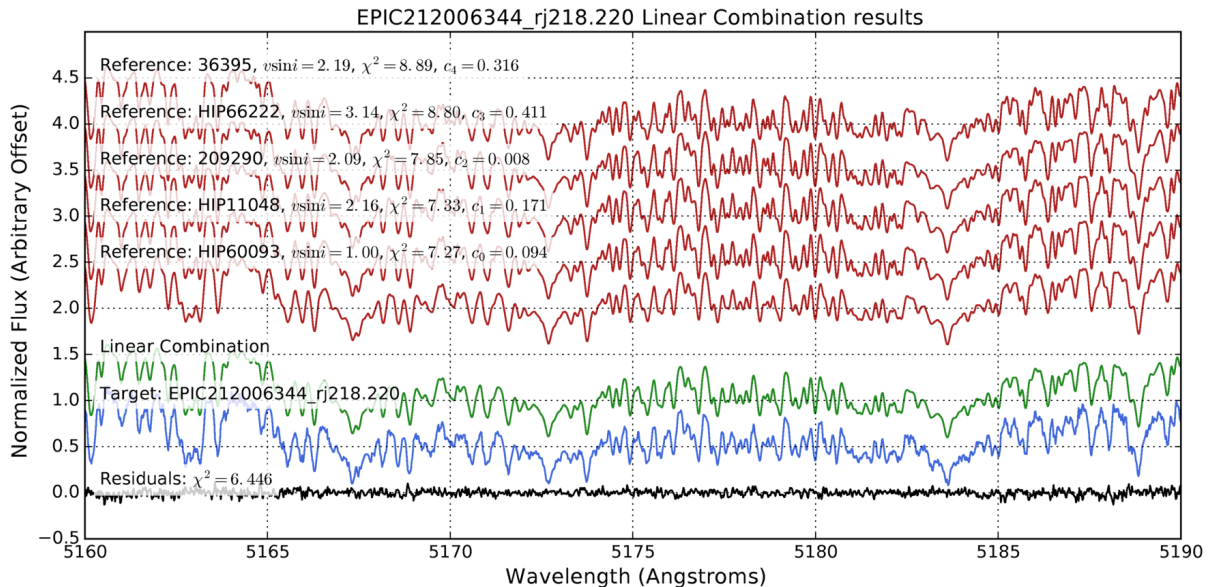
against other spectral synthesis codes, there are known offsets between spectroscopic $T_{\rm eff}$ and other techniques such as the Infrared Flux Method (IRFM) and interferometry. For a detailed discussion of different $T_{\rm eff}$ scales, see Brewer et al. (2016). To account for systematic uncertainties associated with the spectroscopic $T_{\rm eff}$ scale, we have increased the $T_{\rm eff}$ uncertainties to 100 K during the isochrone modeling.

The radius uncertainties derived from `SpecMatch-Syn` parameters do not incorporate uncertainties associated with the MIST models themselves. Johnson et al. (2017) estimated the size of these model-dependent uncertainties through a comparison of stellar radii derived using MIST models and Dartmouth Stellar Evolution Program (DSEP) models (Dotter et al. 2008) with identical inputs. They estimated that model-dependent radius errors are $\approx 2\%$ for dwarf stars ($\log g < 3.9$) and $\approx 10\%$ for evolved stars ($\log g > 3.9$). These model-dependent uncertainties are typically smaller than the formal radius uncertainties returned by `isoclassify`.

For $T_{\rm eff} \lesssim 4700$ K, `SpecMatch-Syn` does not return reliable parameters, due to the onset of molecular lines that are not well-treated in the Coelho et al. (2005) models. While the high-resolution optical spectra of stars later than $\sim$K4 is challenging to compute directly, their spectra contain a wealth of information, which can be used to constrain stellar properties. `SpecMatch-Emp` circumvents the challenges in spectral synthesis by matching a target spectrum against an empirical spectra library of ≈ 400 touchstone stars with well-known param-

eters measured through other methods such as SED-fitting, interferometry, or the IRFM. `SpecMatch-Emp` interpolates between this library of empirical spectra to find linear combination of library spectra that best reproduces the target spectrum. `SpecMatch-Emp` achieves precisions of 70 K in $T_{\rm eff}$, 10% in $R_\star$, and 0.12 dex in [Fe/H].

We adopt parameters from `SpecMatch-Syn` for stars hotter than 4700 K[13] and `SpecMatch-Emp` for cooler stars. Figure 5 shows the $T_{\rm eff}$ and $R_\star$ for K2OIs with reliable spectroscopic parameters. Our adopted stellar parameters are listed in Table 2. Our team also conducts a parallel characterization of cool stars using NIR spectroscopy. Stellar properties up through campaign 7 are given in Martinez et al. (2017) and Dressing et al. (2017).

3.3. *Searches for Spectroscopic Binaries*

Each HIRES spectrum is methodically searched for secondary spectral lines using the `ReaMatch` algorithm (Kolbl et al. 2015). To identify secondary spectra, each spectrum is first cross-correlated against a set of previously-observed spectra. This catalog has spectra with $T_{\rm eff} = 3500$–6500 K and $\log g = 3.0$–4.5 dex. The best-matching spectrum is subtracted from the target spectrum and the residuals are again cross-correlated with the catalog spectra. `ReaMatch` is sensitive to com-

---

[13] as measured by `SpecMatch-Emp`

panions down to 1% the brightness of the primary having RV offsets $|\Delta v| > 10$ km s^{-1}. Optimized for slowly-rotating FGKM stars, `ReaMatch` is insensitive to SB2s orbiting primaries with $v \sin i > 10$ km s^{-1} or with $T_{\rm eff}$ outside 3500–6500 K. Table 2 lists the results of our SB2 search.

4. PLANET CANDIDATES

We list the 151 planet candidates and 16 likely EBs in Table 1. We compute planetary radius by combining $R_P/R_\star$ measured from the light curve with the best available $R_\star$. For the stars without spectra, we estimate $R_\star$ from broadband photometry, according to the following procedure: we estimate spectral types (SpTs) using tabulated photometric relations (Kraus & Hillenbrand 2007; Pecaut & Mamajek 2013; Rodriguez et al. 2013) and convert SpTs into $R_\star$ based on interferometric studies (Boyajian et al. 2012). These stellar radii are crude and we estimate their typical uncertainties to be ≈40%, typical of errors derived from broadband photometry (Brown et al. 2011).

Figure 6 shows the distribution of the 151 planet candidates in the $P - R_P$ plane. Figure 7 shows 1D histograms of our candidates as a function of P, R_P, and Kp. The median host star is nearly two magnitudes brighter in the *Kepler* bandpass than the median KOI from the prime *Kepler* mission (12.8 mag vs 14.6 mag, Mullally et al. 2015). Our candidates have the following multiplicity distribution: 132 singles, 8 doubles, and 1 triple planet system.

We consulted the NASA Exoplanet Archive (NEA; Akeson et al. 2013)[14] to check whether previous analyses have reported significant numbers of candidates presented in this work. Of the catalogs incorporated into the NEA as of 2017-11-09, Barros et al. (2016; B16 hereafter) and Pope et al. (2016; P16 hereafter) included 10 or more candidates from C5–C8.

B16 reported 172 planet candidates from C1–C6, of which 86 were in C5 and C6. Our catalog contains 107 candidates from C5 and C6. The two catalogs share 49 candidates. There are 58 candidates in our catalog that are not in B16, and there are 37 candidates in B16 that are not in our catalog.

P16 reported 168 planet candidates in C5 and C6. Of these, our catalog includes 73 candidates. There are 34 candidates in our catalog that are not in P16, and there are 95 candidates in P16 that are not in our catalog.

As a final point of comparison, B16 and P16 share 59 candidates. There are 27 candidates in B16 that are not in P16, and there are 109 candidates in P16 that were not in B16. Figure 8 is a Venn diagram that summarizes

the degree of overlap between the various samples.

A detailed analysis of why any particular candidate appeared in one catalog and not another is beyond the scope of this work. Broadly-speaking, the lack perfect overlap likely arises due to differences in photometric extraction algorithms, transit search algorithms, adopted signal-to-noise threshold for candidate status, and vetting diagnostics.

5. SUMMARY

We report 151 planet candidates orbiting 141 stars detected through a systematic search of *K2* photometry from campaigns C5–C8. We also identified 16 likely EBs based on their light curve morphology. We obtained Keck/HIRES optical spectra of 105/141 planet candidate host stars and 8/16 EBs to improve our understanding of host star and planet properties and to search for binary companions.

A small fraction of our planet candidates reside in multi-candidate systems (8 doubles and 1 triple). These systems have a low false positive probability ($\lesssim 1\%$) due to their multiplicity (Lissauer et al. 2012). The remaining 132 candidates are well-vetted and well-characterized planet candidates, but have yet been confirmed or statistically validated. Statistical validation requires a detailed analysis of light curve shape and constraints on the presence of blends from high-resolution imaging. Crossfield et al. (2016) performed such an analysis to validate 104 K2 planet candidates identified during C0–C4. Our team's high contrast imaging followup will be presented in Gonzales et al. *in prep.* An analysis of the false positive probabilities of our candidates will be presented in Livingston et al. *in prep.*

Our typical candidate is two magnitudes brighter than the typical candidate from the *Kepler* prime mission due to the larger region of sky observed by *K2*. As a result, these candidates make up a valuable sample for further characterization efforts, such as Doppler measurements of planet masses.

Software: batman (Kreidberg 2015), SpecMatch-Syn (Petigura 2015), SpecMatch-Emp (Yee et al. 2017), k2phot (https://github.com/petigura/k2phot), isoclassify (Huber et al. 2017), isochrones (Morton 2015).

---

[14] https://exoplanetarchive.ipac.caltech.edu/

EPIC212006344_rj218.220 references used in linear combination
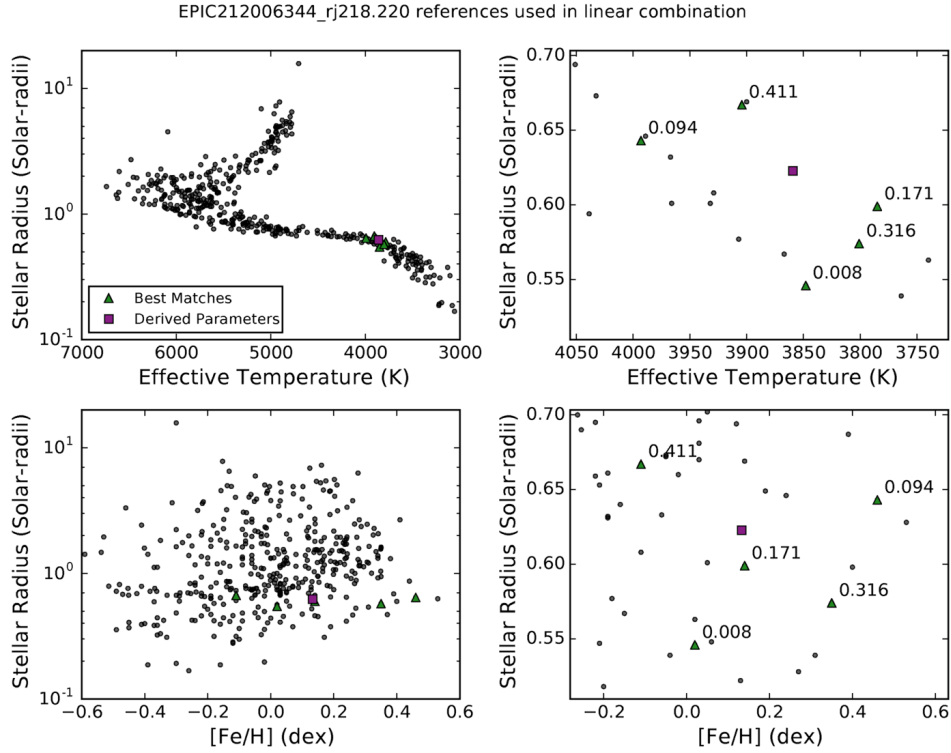
Figure 4. `SpecMatch-Emp` characterization of EPIC212006344. Black points: $T_{\rm eff}$, $R_\star$, and [Fe/H] from the `SpecMatch-Emp` library. Green triangles: properties of the closest-matching library spectra (red spectra in Figure 3). Purple square: linear combination of library spectra spectra. The final derived parameters are $T_{\rm eff} = 3925 \pm 70$ K, [Fe/H] $= 0.43 \pm 0.12$ dex, $R_\star = 0.63 \pm 0.10$ dex.
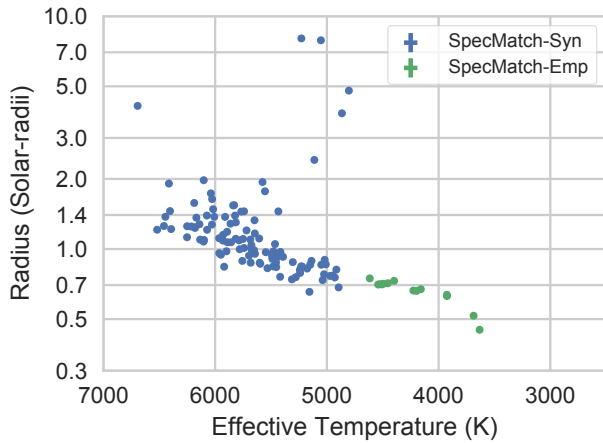
Figure 5. K2OIs with reliable effective temperatures and stellar radii, as measured by `SpecMatch-Syn` (blue) or `SpecMatch-Emp` (green). Median uncertainties are shown at top right.
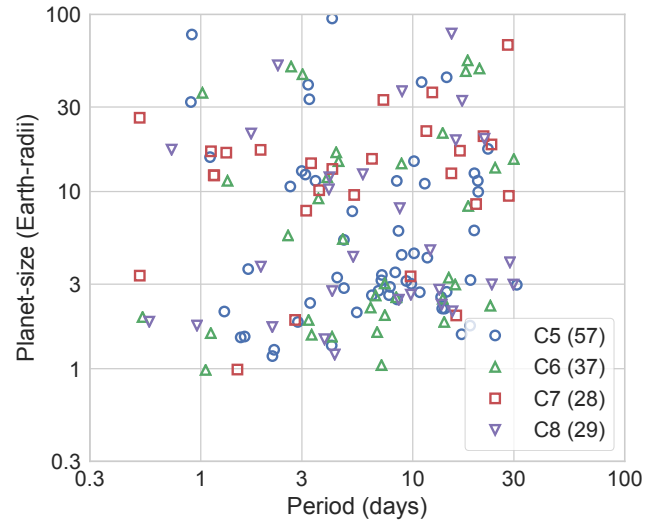
Figure 6. Planet size and orbital period for 151 planet candidates identified by *K2* in C5–C8. We have excluded targets identified as likely EBs from their light curve morphology. The legend at lower right links marker shape/color to a specific campaign and gives the total number of candidates identified in each campaign.
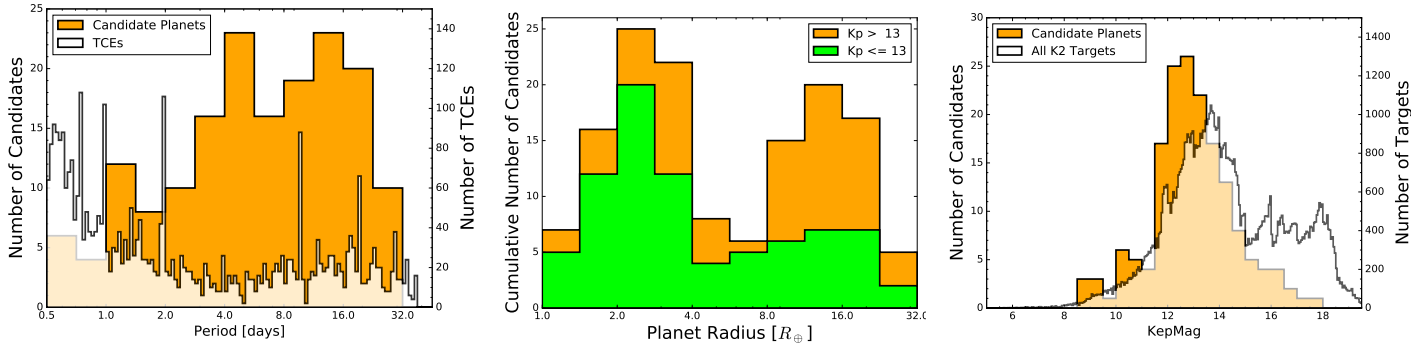
Figure 7. *Left:* Orbital periods of transit-like signals identified in our analysis. The orange histogram (axis at left) indicates the distribution of planet candidates. The pale, narrow-binned histogram (axis at right) indicates the Threshold-Crossing Events (TCEs) identified by TERRA in our initial transit search with MES ≥ 10. *Middle:* Cumulative histograms of radii for our planet candidates. Most are moderately bright at $Kp \leq 13$ mag, but at large radii over half orbit fainter stars; a large fraction of this second group are likely false positives. *Right:* The orange histogram (axis at left) shows the distribution of Kp for planet candidates. For comparison, the pale histogram (axis at right) shows all target stars from C5–C8.
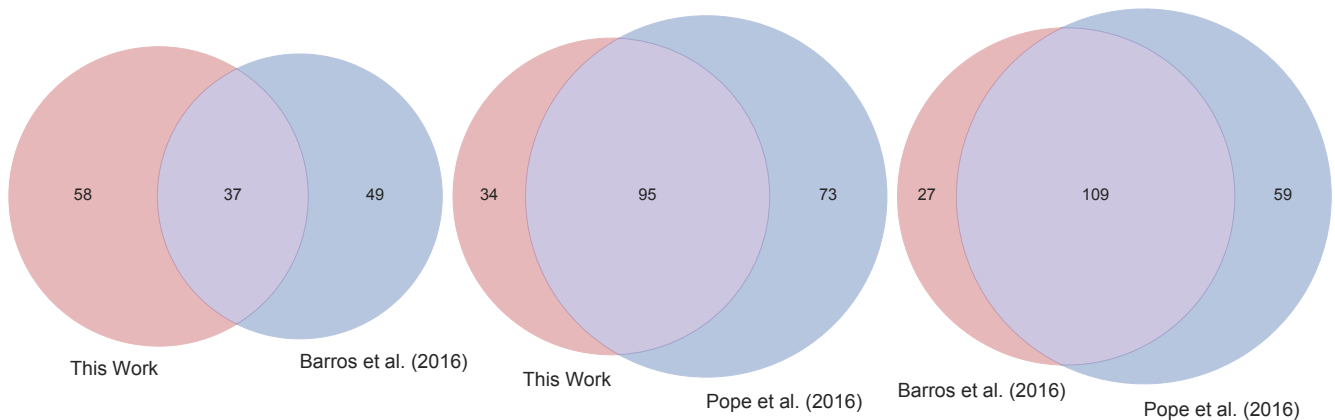
Figure 8. Venn diagrams that compare the candidates from C5 and C6 reported in the following catalogs: This work, Barros et al. (2016), and Pope et al. (2016).

REFERENCES

Aigrain, S., Hodgkin, S. T., Irwin, M. J., Lewis, J. R., & Roberts, S. J. 2015, MNRAS, 447, 2880

Akeson, R. L., Chen, X., Ciardi, D., et al. 2013, PASP, 125, 989

Barros, S. C. C., Demangeon, O., & Deleuil, M. 2016, A&A, 594, A100

Borucki, W. J., Koch, D., Basri, G., et al. 2010, Science, 327, 977

Boyajian, T. S., von Braun, K., van Belle, G., et al. 2012, ApJ, 757, 112

Brewer, J. M., Fischer, D. A., Valenti, J. A., & Piskunov, N. 2016, ApJS, 225, 32

Brown, T. M., Latham, D. W., Everett, M. E., & Esquerdo, G. A. 2011, AJ, 142, 112

Choi, J., Dotter, A., Conroy, C., et al. 2016, ApJ, 823, 102

Christiansen, J. L., Jenkins, J. M., Caldwell, D. A., et al. 2012, PASP, 124, 1279

Coelho, P., Barbuy, B., Meléndez, J., Schiavon, R. P., & Castilho, B. V. 2005, A&A, 443, 735

Crossfield, I. J. M., Petigura, E., Schlieder, J. E., et al. 2015, ApJ, 804, 10

Crossfield, I. J. M., Ciardi, D. R., Petigura, E. A., et al. 2016, ApJS, 226, 7

David, T. J., Hillenbrand, L. A., Petigura, E. A., et al. 2016, Nature, 534, 658

Deming, D., Knutson, H., Kammer, J., et al. 2015, ApJ, 805, 132

Dotter, A., Chaboyer, B., Jevremović, D., et al. 2008, ApJS, 178, 89

Dressing, C. D., & Charbonneau, D. 2015, ApJ, 807, 45

Dressing, C. D., Newton, E. R., Schlieder, J. E., et al. 2017, ApJ, 836, 167

Eastman, J., Gaudi, B. S., & Agol, E. 2013, PASP, 125, 83

Foreman-Mackey, D., Montet, B. T., Hogg, D. W., et al. 2015, ApJ, 806, 215

Goodman, J., & Weare, J. 2010, Communications in Applied Mathematics and Computational Science, 5, 65

Howard, A. W., Sanchis-Ojeda, R., Marcy, G. W., et al. 2013, Nature, 503, 381

Howell, S. B., Sobeck, C., Haas, M., et al. 2014, PASP, 126, 398

Huber, D., Bryson, S. T., Haas, M. R., et al. 2016, ApJS, 224, 2

Huber, D., Zinn, J., Bojsen-Hansen, M., et al. 2017, ArXiv e-prints, arXiv:1705.04697

Johnson, J. A., Petigura, E. A., Fulton, B. J., et al. 2017, AJ, 154, 108

Jontof-Hutter, D., Rowe, J. F., Lissauer, J. J., Fabrycky, D. C., & Ford, E. B. 2015, Nature, 522, 321

Kolbl, R., Marcy, G. W., Isaacson, H., & Howard, A. W. 2015, AJ, 149, 18

Kraus, A. L., & Hillenbrand, L. A. 2007, AJ, 134, 2340

Kreidberg, L. 2015, ArXiv e-prints, arXiv:1507.08285

Lissauer, J. J., Marcy, G. W., Rowe, J. F., et al. 2012, ApJ, 750, 112

Lucy, L. B., & Sweeney, M. A. 1971, AJ, 76, 544

Luger, R., Agol, E., Kruse, E., et al. 2016, AJ, 152, 100

Mann, A. W., Newton, E. R., Rizzuto, A. C., et al. 2016, AJ, 152, 61

Marcy, G. W., Isaacson, H., Howard, A. W., et al. 2014, ApJS, 210, 20

Martinez, A. O., Crossfield, I. J. M., Schlieder, J. E., et al. 2017, ApJ, 837, 72

Montet, B. T., Morton, T. D., Foreman-Mackey, D., et al. 2015, ApJ, 809, 25

Morton, T. D. 2015, isochrones: Stellar model grid package, Astrophysics Source Code Library, , , ascl:1503.010

Mullally, F., Coughlin, J. L., Thompson, S. E., et al. 2015, ApJS, 217, 31

Parviainen, H., & Aigrain, S. 2015, MNRAS, 453, 3821

Paxton, B., Bildsten, L., Dotter, A., et al. 2011, ApJS, 192, 3

Paxton, B., Cantiello, M., Arras, P., et al. 2013, ApJS, 208, 4

Paxton, B., Marchant, P., Schwab, J., et al. 2015, ApJS, 220, 15

Pecaut, M. J., & Mamajek, E. E. 2013, ApJS, 208, 9

Petigura, E. A. 2015, PhD thesis, University of California, Berkeley

Petigura, E. A., Howard, A. W., & Marcy, G. W. 2013, Proceedings of the National Academy of Science, 110, 19273

Petigura, E. A., Schlieder, J. E., Crossfield, I. J. M., et al. 2015, ApJ, 811, 102

Petigura, E. A., Howard, A. W., Marcy, G. W., et al. 2017, AJ, 154, 107

Pope, B. J. S., Parviainen, H., & Aigrain, S. 2016, MNRAS, 461, 3399

Rodriguez, D. R., Zuckerman, B., Kastner, J. H., et al. 2013, ApJ, 774, 101

Rogers, L. A. 2015, ApJ, 801, 41

Schlieder, J. E., Crossfield, I. J. M., Petigura, E. A., et al. 2016, ApJ, 818, 87

Storn, R., & Price, K. 1997, Journal of Global Optimization, 11, 341

Vanderburg, A., & Johnson, J. A. 2014, PASP, 126, 948

Vanderburg, A., Johnson, J. A., Rappaport, S., et al. 2015, Nature, 526, 546

Vogt, S. S., Allen, S. L., Bigelow, B. C., et al. 1994, 2198, 362

Weiss, L. M., & Marcy, G. W. 2014, ApJL, 783, L6

Yee, S. W., Petigura, E. A., & von Braun, K. 2017, ApJ, 836, 77

APPENDIX

Table 1. Planet Candidates

	Cand.	Kp mag	$R_\star$ $R_\odot$	Prov.	P days	$R_P/R_\star$ %	T_{14} hr	b	R_P $R_\oplus$	EB	Comments
C5	211401787.01	9.7	1.25	S	13.8	$1.60^{+0.13}_{-0.06}$	$4.54^{+0.13}_{-0.12}$	$0.43^{+0.32}_{-0.30}$	$2.2^{+0.4}_{-0.2}$	0	
C5	211945201.01	10.1	1.48	S	19.5	$3.73^{+0.23}_{-0.08}$	$3.58^{+0.12}_{-0.05}$	$0.46^{+0.28}_{-0.32}$	$6.0^{+0.9}_{-0.8}$	0	
C5	211990866.01	10.4	1.23	S	1.7	$2.72^{+0.26}_{-0.10}$	$1.54^{+0.05}_{-0.05}$	$0.46^{+0.32}_{-0.32}$	$3.6^{+0.4}_{-0.2}$	0	∼1% spot modulation
C5	212099230.01	10.5	0.96	S	7.1	$3.02^{+0.11}_{-0.10}$	$3.13^{+0.05}_{-0.06}$	$0.97^{+0.01}_{-0.01}$	$3.2^{+0.3}_{-0.2}$	0	
C5	211594205.01	10.7	0.79	S	17.0	$1.82^{+0.24}_{-0.10}$	$2.49^{+0.11}_{-0.09}$	$0.48^{+0.30}_{-0.33}$	$1.6^{+0.2}_{-0.1}$	0	
C5	212110888.01	11.4	1.38	S	3.0	$8.70^{+0.05}_{-0.05}$	$2.36^{+0.01}_{-0.02}$	$0.77^{+0.01}_{-0.01}$	$13.1^{+1.8}_{-1.6}$	0	
C5	211525389.01	11.7	0.98	S	8.3	$3.28^{+0.19}_{-0.07}$	$3.40^{+0.06}_{-0.05}$	$0.38^{+0.29}_{-0.27}$	$3.5^{+0.4}_{-0.2}$	0	
C5	211359660.01	11.7	0.82	S	4.7	$3.17^{+0.18}_{-0.06}$	$2.57^{+0.04}_{-0.03}$	$0.34^{+0.30}_{-0.24}$	$2.9^{+0.2}_{-0.1}$	0	
C5	212012119.01	11.8	0.75	S	3.3	$2.85^{+0.29}_{-0.12}$	$1.93^{+0.05}_{-0.04}$	$0.43^{+0.30}_{-0.29}$	$2.3^{+0.3}_{-0.1}$	0	
C5	212012119.02	11.8	0.75	S	8.4	$2.99^{+0.36}_{-0.14}$	$2.34^{+0.08}_{-0.06}$	$0.48^{+0.29}_{-0.32}$	$2.5^{+0.3}_{-0.1}$	0	
C5	211491383.01	11.8	1.28	S	4.1	$0.97^{+0.13}_{-0.07}$	$2.71^{+0.23}_{-0.21}$	$0.50^{+0.33}_{-0.33}$	$1.4^{+0.3}_{-0.2}$	0	
C5	211391664.01	12.1	1.39	S	10.1	$2.95^{+0.12}_{-0.06}$	$4.97^{+0.11}_{-0.09}$	$0.38^{+0.29}_{-0.26}$	$4.5^{+0.6}_{-0.5}$	0	
C5	211736671.01	12.2	1.77	S	4.7	$2.76^{+0.18}_{-0.07}$	$3.55^{+0.07}_{-0.06}$	$0.41^{+0.30}_{-0.28}$	$5.3^{+0.9}_{-0.7}$	0	
C5	212066407.01	12.2	1.07	S	0.8	$2.22^{+0.21}_{-0.09}$	$0.83^{+0.05}_{-0.05}$	$0.51^{+0.32}_{-0.35}$	$2.6^{+0.4}_{-0.3}$	2	
C5	211319617.01	12.4	0.65	S	8.9	$6.15^{+8.29}_{-2.79}$	$0.30^{+1.18}_{-0.20}$	$0.63^{+0.38}_{-0.43}$	$4.4^{+5.9}_{-2.0}$	0	
C5	211342524.01	12.4	1.36	S	14.4	$29.69^{+11.04}_{-4.64}$	$3.75^{+0.02}_{-0.02}$	$0.98^{+0.14}_{-0.07}$	$44.2^{+17.5}_{-8.6}$	0	Deep (3%); V-shaped
C5	211351816.01	12.4	4.79	S	8.4	$2.20^{+0.35}_{-0.16}$	$5.72^{+0.28}_{-0.27}$	$0.52^{+0.31}_{-0.35}$	$11.5^{+2.8}_{-1.8}$	0	
C5	211800191.01	12.4	0.84	S	1.1	$17.08^{+24.11}_{-11.25}$	$0.00^{+0.53}_{-0.00}$	$1.25^{+0.36}_{-0.20}$	$15.6^{+22.1}_{-10.3}$	0	V-shaped

Table 1 *(continued)*

	Cand.	Kp	$R_\star$	Prov.	P	$R_P/R_\star$	T_{14}	b	R_P	EB	Comments
		mag	$R_\odot$		days	%	hr		$R_\oplus$		
C5	212006344.01	12.5	0.63	S	2.2	$1.87^{+0.24}_{-0.11}$	$1.27^{+0.09}_{-0.09}$	$0.50^{+0.32}_{-0.34}$	$1.3^{+0.3}_{-0.2}$	0	
C5	211355342.01	12.6	1.11	S	6.9	$2.28^{+0.21}_{-0.13}$	$2.44^{+0.15}_{-0.16}$	$0.49^{+0.31}_{-0.34}$	$2.8^{+0.4}_{-0.3}$	0	
C5	212164470.01	12.7	1.19	S	7.8	$2.24^{+0.25}_{-0.11}$	$3.58^{+0.14}_{-0.13}$	$0.46^{+0.32}_{-0.30}$	$2.9^{+0.5}_{-0.3}$	0	
C5	211562654.01	12.8	0.92	S	10.8	$2.68^{+0.24}_{-0.10}$	$3.85^{+0.16}_{-0.14}$	$0.47^{+0.31}_{-0.32}$	$2.7^{+0.3}_{-0.2}$	0	Multi
C5	211562654.02	12.8	0.92	S	22.6	$17.29^{+42.34}_{-13.31}$	$4.14^{+0.45}_{-0.17}$	$1.14^{+0.44}_{-0.96}$	$17.4^{+42.7}_{-13.4}$	0	Multi
C5	212008766.01	12.8	0.74	S	14.1	$2.72^{+0.31}_{-0.12}$	$3.23^{+0.18}_{-0.15}$	$0.50^{+0.32}_{-0.34}$	$2.2^{+0.3}_{-0.1}$	0	
C5	212157262.01	12.9	0.96	S	7.1	$3.24^{+0.45}_{-0.16}$	$2.84^{+0.18}_{-0.12}$	$0.55^{+0.32}_{-0.38}$	$3.4^{+0.5}_{-0.2}$	0	Multi
C5	212157262.02	12.9	0.96	S	13.6	$2.43^{+0.26}_{-0.13}$	$4.03^{+0.26}_{-0.24}$	$0.49^{+0.32}_{-0.33}$	$2.5^{+0.3}_{-0.2}$	0	Multi
C5	212157262.03	12.9	0.96	S	2.9	$1.76^{+0.21}_{-0.13}$	$2.19^{+0.25}_{-0.24}$	$0.52^{+0.32}_{-0.35}$	$1.8^{+0.3}_{-0.2}$	0	Multi
C5	212138198.01	12.9	0.89	S	3.2	$41.32^{+37.69}_{-27.13}$	$0.84^{+0.08}_{-0.09}$	$1.36^{+0.39}_{-0.30}$	$40.1^{+36.7}_{-26.4}$	0	V-shaped
C5	211818569.01	12.9	0.71	S	5.2	$10.05^{+0.13}_{-0.05}$	$2.03^{+0.01}_{-0.01}$	$0.14^{+0.14}_{-0.10}$	$7.7^{+1.1}_{-1.1}$	0	
C5	211439059.01	13.1	0.84	S	18.6	$1.91^{+0.30}_{-0.16}$	$5.06^{+0.49}_{-0.46}$	$0.51^{+0.32}_{-0.34}$	$1.8^{+0.3}_{-0.2}$	0	
C5	211919004.01	13.1	0.86	S	11.7	$4.54^{+2.89}_{-0.43}$	$5.19^{+0.19}_{-0.36}$	$0.96^{+0.06}_{-0.04}$	$4.2^{+2.7}_{-0.4}$	0	
C5	211442297.01	13.2	0.86	S	20.3	$12.21^{+0.18}_{-0.21}$	$3.70^{+0.06}_{-0.07}$	$0.47^{+0.08}_{-0.15}$	$11.5^{+0.8}_{-0.6}$	0	
C5	211428897.01	13.2	0.56	P	1.6	$2.49^{+0.38}_{-0.16}$	$1.07^{+0.07}_{-0.06}$	$0.53^{+0.31}_{-0.35}$	$1.5^{+0.7}_{-0.6}$	0	Multi
C5	211428897.02	13.2	0.56	P	2.2	$1.93^{+0.30}_{-0.15}$	$1.29^{+0.14}_{-0.13}$	$0.52^{+0.32}_{-0.35}$	$1.2^{+0.5}_{-0.5}$	0	Multi
C5	211490999.01	13.4	0.91	S	9.8	$3.05^{+0.32}_{-0.11}$	$3.63^{+0.16}_{-0.10}$	$0.51^{+0.31}_{-0.34}$	$3.0^{+0.4}_{-0.2}$	0	
C5	211529065.01	13.4	0.82	S	4.4	$3.68^{+0.52}_{-0.20}$	$1.56^{+0.07}_{-0.06}$	$0.48^{+0.30}_{-0.32}$	$3.3^{+0.5}_{-0.4}$	0	Multi
C5	211529065.02	13.4	0.82	S	1.5	$1.69^{+0.28}_{-0.14}$	$1.76^{+0.16}_{-0.18}$	$0.51^{+0.33}_{-0.35}$	$1.5^{+0.3}_{-0.1}$	0	Multi
C5	211413752.01	13.5	0.78	S	9.3	$3.68^{+5.79}_{-0.63}$	$2.81^{+0.36}_{-0.31}$	$0.81^{+0.24}_{-0.53}$	$3.1^{+4.9}_{-0.5}$	0	
C5	211713099.01	13.6	0.83	S	8.6	$6.65^{+0.18}_{-0.07}$	$3.24^{+0.03}_{-0.02}$	$0.23^{+0.19}_{-0.16}$	$6.0^{+0.4}_{-0.3}$	0	
C5	211816003.01	13.7	0.74	S	14.5	$3.36^{+0.41}_{-0.19}$	$3.47^{+0.19}_{-0.16}$	$0.48^{+0.30}_{-0.31}$	$2.7^{+0.4}_{-0.2}$	0	
C5	211331236.01	13.9	0.52	S	1.3	$3.73^{+0.41}_{-0.17}$	$1.19^{+0.07}_{-0.07}$	$0.47^{+0.33}_{-0.32}$	$2.1^{+0.5}_{-0.4}$	0	Multi
C5	211331236.02	13.9	0.52	S	5.4	$3.69^{+0.38}_{-0.20}$	$2.18^{+0.17}_{-0.15}$	$0.47^{+0.31}_{-0.32}$	$2.1^{+0.5}_{-0.4}$	0	Multi
C5	212069861.01	14.1	0.64	S	31.0	$4.29^{+0.52}_{-0.22}$	$3.76^{+0.20}_{-0.16}$	$0.43^{+0.29}_{-0.29}$	$3.0^{+0.6}_{-0.5}$	0	
C5	211929937.01	14.2	0.84	S	3.5	$12.52^{+0.10}_{-0.05}$	$2.54^{+0.01}_{-0.01}$	$0.11^{+0.11}_{-0.08}$	$11.5^{+0.6}_{-0.5}$	0	
C5	211418729.01	14.3	0.90	S	11.4	$11.31^{+0.24}_{-0.11}$	$3.83^{+0.04}_{-0.03}$	$0.20^{+0.16}_{-0.13}$	$11.1^{+0.8}_{-0.6}$	0	
C5	211578235.01	14.3	0.94	S	11.0	$40.56^{+37.66}_{-25.60}$	$1.54^{+0.07}_{-0.07}$	$1.29^{+0.39}_{-0.30}$	$41.5^{+39.0}_{-26.4}$	0	
C5	211399359.01	14.4	0.77	S	3.1	$14.93^{+0.13}_{-0.06}$	$2.36^{+0.01}_{-0.01}$	$0.10^{+0.10}_{-0.07}$	$12.5^{+0.5}_{-0.4}$	0	
C5	211978865.01	14.4	1.21	S	0.9	$58.31^{+29.46}_{-27.44}$	$0.00^{+0.94}_{-0.00}$	$1.69^{+0.45}_{-0.41}$	$77.0^{+39.8}_{-36.6}$	0	
C5	212130773.01	14.5	0.77	S	18.7	$3.78^{+0.43}_{-0.23}$	$6.48^{+0.29}_{-0.28}$	$0.42^{+0.29}_{-0.29}$	$3.2^{+0.4}_{-0.2}$	0	
C5	211770795.01	14.5	0.71	S	7.7	$3.35^{+0.61}_{-0.27}$	$2.84^{+0.25}_{-0.23}$	$0.52^{+0.32}_{-0.35}$	$2.6^{+0.6}_{-0.4}$	0	
C5	212150006.01	14.7	0.79	P	0.9	$37.28^{+30.56}_{-24.31}$	$0.00^{+0.00}_{-0.00}$	$1.58^{+0.47}_{-0.40}$	$32.0^{+29.2}_{-24.5}$	0	V-shaped
C5	211924657.01	15.0	0.50	P	2.6	$19.51^{+43.78}_{-13.30}$	$1.53^{+0.25}_{-1.53}$	$1.13^{+0.52}_{-0.29}$	$10.7^{+24.3}_{-8.4}$	0	
C5	212154564.01	15.1	0.35	P	6.4	$6.76^{+0.70}_{-0.27}$	$1.75^{+0.09}_{-0.07}$	$0.36^{+0.29}_{-0.25}$	$2.6^{+1.1}_{-1.0}$	0	
C5	211916756.01	15.5	0.43	P	10.1	$31.61^{+43.78}_{-23.33}$	$3.37^{+0.28}_{-0.43}$	$1.20^{+0.47}_{-0.45}$	$14.8^{+21.4}_{-12.5}$	0	
C5	211509553.01	15.7	0.53	P	20.4	$17.30^{+0.22}_{-0.12}$	$3.59^{+0.03}_{-0.03}$	$0.12^{+0.11}_{-0.08}$	$10.0^{+4.0}_{-4.0}$	0	
C5	211799258.01	16.0	0.45	P	19.5	$25.93^{+6.68}_{-1.29}$	$1.29^{+0.07}_{-0.05}$	$0.43^{+0.34}_{-0.29}$	$12.7^{+6.0}_{-5.1}$	0	Deep (8%); V-shaped
C5	211831378.01	16.3	0.28	P	3.5	$51.67^{+29.86}_{-27.70}$	$2.12^{+0.38}_{-0.66}$	$1.45^{+0.34}_{-0.32}$	$15.6^{+10.9}_{-10.4}$	1	
C5	211910968.01	16.5	0.23	P	4.5	$18.62^{+0.19}_{-0.14}$	$5.20^{+0.04}_{-0.04}$	$0.09^{+0.10}_{-0.06}$	$4.7^{+1.9}_{-1.9}$	1	Eccentric EB; depth uncertain
C5	211413463.01	17.3	0.63	P	3.3	$48.64^{+27.21}_{-18.79}$	$2.72^{+0.20}_{-0.40}$	$1.37^{+0.31}_{-0.22}$	$33.2^{+22.8}_{-18.5}$	0	Transit likely due to nearby star; depth uncertain
C5	211375488.01	17.5	2.00	P	4.2	$43.48^{+36.92}_{-27.97}$	$2.73^{+0.19}_{-0.20}$	$1.26^{+0.40}_{-0.35}$	$94.8^{+89.0}_{-71.8}$	0	
C6	212727070.01	9.4	1.15	P	15.5	$54.40^{+17.34}_{-11.88}$	$6.14^{+0.06}_{-0.05}$	$1.14^{+0.19}_{-0.16}$	$68.4^{+35.0}_{-31.2}$	1	
C6	212357477.01	10.2	1.01	S	6.3	$2.01^{+0.27}_{-0.12}$	$1.83^{+0.10}_{-0.09}$	$0.50^{+0.31}_{-0.34}$	$2.2^{+0.4}_{-0.2}$	0	
C6	212351868.01	10.2	0.94	P	2.5	$24.46^{+0.07}_{-0.05}$	$5.63^{+0.02}_{-0.01}$	$0.07^{+0.06}_{-0.05}$	$25.1^{+10.1}_{-10.1}$	1	
C6	212651120.01	10.5	1.08	P	0.7	$1.39^{+0.04}_{-0.03}$	$4.69^{+0.27}_{-0.95}$	$0.53^{+0.27}_{-0.33}$	$1.6^{+0.7}_{-0.7}$	2	
C6	212703473.01	10.7	1.11	S	6.8	$1.33^{+0.19}_{-0.11}$	$2.77^{+0.27}_{-0.28}$	$0.50^{+0.32}_{-0.34}$	$1.6^{+0.3}_{-0.2}$	0	
C6	212803289.01	11.0	1.98	S	18.3	$3.85^{+0.13}_{-0.07}$	$11.05^{+0.16}_{-0.11}$	$0.38^{+0.23}_{-0.25}$	$8.3^{+1.3}_{-1.2}$	0	

Table 1 continued

Table 1 *(continued)*

	Cand.	Kp	$R_\star$	Prov.	P	$R_P/R_\star$	T_{14}	b	R_P	EB	Comments
		mag	$R_\odot$		days	%	hr		$R_\oplus$		
C6	212773309.01	11.4	0.86	S	4.7	$24.44^{+0.29}_{-0.28}$	$2.28^{+0.02}_{-0.02}$	$0.69^{+0.02}_{-0.02}$	$22.9^{+1.3}_{-1.0}$	1	
C6	212577658.01	11.5	0.84	P	14.1	$2.01^{+0.29}_{-0.12}$	$2.99^{+0.12}_{-0.12}$	$0.49^{+0.30}_{-0.33}$	$1.8^{+0.8}_{-0.7}$	0	
C6	212782836.01	11.6	0.76	S	7.1	$1.26^{+0.17}_{-0.09}$	$3.14^{+0.26}_{-0.25}$	$0.49^{+0.32}_{-0.33}$	$1.0^{+0.1}_{-0.1}$	0	low SNR
C6	212521166.01	11.6	0.68	S	13.9	$3.33^{+0.22}_{-0.08}$	$3.20^{+0.06}_{-0.05}$	$0.41^{+0.28}_{-0.27}$	$2.5^{+0.2}_{-0.1}$	0	
C6	212586030.01	11.7	3.83	S	7.8	$37.28^{+39.24}_{-26.58}$	$1.26^{+0.52}_{-1.26}$	$1.36^{+0.41}_{-0.29}$	$155.7^{+165.8}_{-113.0}$	0	
C6	212300977.01	11.7	1.11	S	4.5	$12.23^{+0.04}_{-0.02}$	$3.52^{+0.01}_{-0.01}$	$0.07^{+0.07}_{-0.05}$	$14.8^{+1.7}_{-1.2}$	0	
C6	212779596.01	11.9	0.70	S	7.4	$3.94^{+0.45}_{-0.16}$	$2.45^{+0.11}_{-0.08}$	$0.48^{+0.31}_{-0.33}$	$3.0^{+0.6}_{-0.4}$	0	Multi
C6	212779596.02	11.9	0.70	S	3.2	$2.45^{+0.32}_{-0.13}$	$2.04^{+0.10}_{-0.10}$	$0.52^{+0.31}_{-0.35}$	$1.9^{+0.4}_{-0.3}$	0	Multi
C6	212735333.01	12.0	0.96	S	8.4	$2.41^{+0.32}_{-0.15}$	$3.47^{+0.19}_{-0.18}$	$0.49^{+0.31}_{-0.33}$	$2.5^{+0.4}_{-0.2}$	0	
C6	212679181.01	12.0	0.36	P	1.1	$2.49^{+0.33}_{-0.17}$	$0.49^{+0.06}_{-0.05}$	$0.50^{+0.33}_{-0.34}$	$1.0^{+0.4}_{-0.4}$	0	
C6	212587672.01	12.2	0.95	S	23.2	$2.20^{+0.26}_{-0.13}$	$3.23^{+0.19}_{-0.16}$	$0.49^{+0.32}_{-0.34}$	$2.3^{+0.3}_{-0.2}$	0	
C6	212697709.01	12.2	1.20	S	4.0	$9.17^{+0.11}_{-0.11}$	$1.83^{+0.02}_{-0.03}$	$0.85^{+0.01}_{-0.01}$	$12.0^{+1.7}_{-1.3}$	0	WASP-157b
C6	212394689.01	12.2	0.88	S	6.7	$2.71^{+0.22}_{-0.09}$	$2.71^{+0.09}_{-0.08}$	$0.46^{+0.30}_{-0.31}$	$2.6^{+0.3}_{-0.2}$	0	
C6	212689874.01	12.3	0.95	S	15.9	$2.87^{+0.16}_{-0.08}$	$4.84^{+0.14}_{-0.12}$	$0.39^{+0.31}_{-0.27}$	$3.0^{+0.4}_{-0.2}$	0	
C6	212435047.01	12.4	1.10	S	1.1	$1.32^{+0.19}_{-0.10}$	$1.58^{+0.21}_{-0.23}$	$0.52^{+0.34}_{-0.35}$	$1.6^{+0.3}_{-0.2}$	0	V-shaped; low SNR
C6	212460519.01	12.4	0.66	S	7.4	$2.78^{+0.31}_{-0.13}$	$2.63^{+0.09}_{-0.08}$	$0.48^{+0.28}_{-0.32}$	$2.0^{+0.4}_{-0.3}$	0	
C6	212639319.01	12.5	0.81	P	13.8	$24.21^{+44.69}_{-19.27}$	$1.77^{+0.19}_{-0.18}$	$1.20^{+0.46}_{-0.22}$	$21.4^{+40.4}_{-19.1}$	0	
C6	212555594.02	12.5	0.83	P	4.2	$1.68^{+0.26}_{-0.17}$	$1.55^{+0.20}_{-0.20}$	$0.50^{+0.32}_{-0.34}$	$1.5^{+0.7}_{-0.6}$	0	212555594.01 is due to noise, 212555594.02 looks transit llke
C6	212428509.01	12.5	0.94	S	2.7	$49.70^{+8.63}_{-8.53}$	$2.09^{+0.16}_{-0.19}$	$1.42^{+0.10}_{-0.10}$	$50.7^{+11.9}_{-9.7}$	0	Deep (1%); V-shaped
C6	212585579.01	12.6	1.09	S	3.0	$38.76^{+35.69}_{-24.16}$	$0.00^{+0.00}_{-0.00}$	$1.45^{+0.44}_{-0.30}$	$45.9^{+42.6}_{-28.9}$	0	V-shaped
C6	212691727.01	12.7	0.87	P	12.9	$23.20^{+0.65}_{-0.49}$	$4.97^{+0.06}_{-0.05}$	$0.19^{+0.14}_{-0.13}$	$22.1^{+8.8}_{-8.8}$	1	
C6	212572439.01	12.8	0.78	P	2.6	$6.68^{+0.40}_{-0.32}$	$1.69^{+0.07}_{-0.04}$	$0.60^{+0.16}_{-0.29}$	$5.7^{+2.3}_{-2.3}$	0	EPIC-212572452 (Kp = 14.8) in photometric aperture
C6	212756297.01	13.0	0.66	P	1.3	$15.99^{+0.02}_{-0.01}$	$1.85^{+0.00}_{-0.00}$	$0.03^{+0.04}_{-0.02}$	$11.5^{+4.6}_{-4.6}$	0	
C6	212580872.01	13.0	0.83	P	14.8	$3.59^{+0.16}_{-0.08}$	$4.32^{+0.09}_{-0.07}$	$0.34^{+0.27}_{-0.23}$	$3.3^{+1.3}_{-1.3}$	0	
C6	212797028.01	13.1	0.94	P	30.0	$14.81^{+0.36}_{-0.24}$	$6.37^{+0.06}_{-0.06}$	$0.85^{+0.01}_{-0.01}$	$15.3^{+6.1}_{-6.1}$	0	Deep ($\sim$2%); V-shaped
C6	212443457.01	13.1	0.68	P	24.5	$18.42^{+29.25}_{-6.81}$	$8.49^{+0.18}_{-0.21}$	$1.02^{+0.34}_{-0.11}$	$13.6^{+22.3}_{-7.4}$	0	Deep (1%); irregular transit shape; possible heirarchical triple
C6	212432685.01	13.1	1.06	P	0.5	$1.69^{+0.18}_{-0.09}$	$1.59^{+0.12}_{-0.22}$	$0.48^{+0.37}_{-0.33}$	$2.0^{+0.8}_{-0.8}$	0	
C6	212294561.01	13.1	0.85	P	2.8	$21.48^{+36.05}_{-16.50}$	$0.00^{+0.00}_{-0.00}$	$1.39^{+0.54}_{-0.29}$	$19.9^{+34.3}_{-17.2}$	1	
C6	212418133.01	13.2	0.90	P	3.3	$1.59^{+0.23}_{-0.13}$	$3.48^{+0.31}_{-0.34}$	$0.48^{+0.33}_{-0.33}$	$1.6^{+0.7}_{-0.6}$	0	
C6	212628098.01	13.3	0.67	P	4.4	$22.72^{+0.52}_{-0.49}$	$1.63^{+0.03}_{-0.03}$	$0.64^{+0.04}_{-0.05}$	$16.6^{+6.7}_{-6.7}$	0	Deep ($\sim$5%); V-shaped; spot mod.
C6	212839127.01	13.3	1.05	P	20.6	$43.10^{+21.49}_{-11.79}$	$4.03^{+0.02}_{-0.02}$	$1.11^{+0.24}_{-0.15}$	$49.5^{+31.6}_{-24.0}$	0	Deep ($\sim$5%); V-shaped;
C6	212579164.01	13.6	0.83	P	18.2	$60.70^{+14.10}_{-8.51}$	$3.59^{+0.08}_{-0.07}$	$0.74^{+0.18}_{-0.15}$	$55.0^{+25.4}_{-23.3}$	0	V-shaped; Deep ($\sim$20%)
C6	212751916.01	13.9	0.90	P	15.7	$24.26^{+46.48}_{-19.77}$	$2.71^{+0.54}_{-0.47}$	$1.19^{+0.48}_{-0.41}$	$23.7^{+46.4}_{-21.5}$	1	
C6	212570977.01	13.9	0.87	P	8.9	$15.14^{+0.10}_{-0.10}$	$4.22^{+0.03}_{-0.03}$	$0.43^{+0.04}_{-0.05}$	$14.4^{+5.8}_{-5.8}$	0	
C6	212757039.01	14.4	0.80	P	4.5	$16.06^{+0.09}_{-0.09}$	$3.34^{+0.02}_{-0.02}$	$0.79^{+0.01}_{-0.01}$	$14.0^{+5.6}_{-5.6}$	1	
C6	212311834.01	14.7	0.76	P	17.8	$57.91^{+21.67}_{-15.49}$	$2.81^{+0.02}_{-0.02}$	$1.06^{+0.25}_{-0.21}$	$47.8^{+26.2}_{-23.0}$	0	V-shaped; Deep ($\sim$10%)
C6	212554013.01	14.7	0.75	P	3.6	$11.17^{+0.38}_{-0.21}$	$2.19^{+0.06}_{-0.03}$	$0.37^{+0.19}_{-0.24}$	$9.1^{+3.7}_{-3.7}$	0	
C6	212679798.01	14.8	0.67	P	1.8	$36.83^{+31.79}_{-7.89}$	$2.19^{+0.04}_{-0.03}$	$0.86^{+0.41}_{-0.17}$	$27.1^{+25.8}_{-12.3}$	1	
C6	212773272.01	15.0	0.25	P	4.7	$19.87^{+1.00}_{-0.68}$	$2.05^{+0.14}_{-0.11}$	$0.32^{+0.25}_{-0.22}$	$5.4^{+2.2}_{-2.2}$	0	Deep ($\sim$5%);
C6	212421319.01	16.4	0.80	P	5.5	$54.69^{+31.61}_{-28.57}$	$7.01^{+0.99}_{-2.08}$	$1.41^{+0.38}_{-0.38}$	$48.0^{+33.7}_{-31.6}$	1	
C6	212757601.01	16.8	0.75	P	1.0	$43.93^{+34.93}_{-24.84}$	$0.96^{+0.63}_{-0.96}$	$1.40^{+0.48}_{-0.36}$	$36.1^{+32.1}_{-25.0}$	0	
C7	218541396.01	10.0	1.18	P	1.0	$52.48^{+29.45}_{-25.10}$	$0.00^{+1.21}_{-0.00}$	$1.61^{+0.46}_{-0.39}$	$67.3^{+46.4}_{-42.0}$	1	Deep ($\sim$2%); V-shaped;
C7	213920015.01	10.0	0.87	S	1.5	$1.04^{+0.09}_{-0.05}$	$1.46^{+0.10}_{-0.12}$	$0.50^{+0.33}_{-0.34}$	$1.0^{+0.1}_{-0.1}$	0	
C7	218711655.01	11.3	1.46	S	1.2	$7.77^{+4.84}_{-3.24}$	$0.00^{+0.00}_{-0.00}$	$1.29^{+0.10}_{-0.11}$	$12.3^{+7.9}_{-5.3}$	0	2 stars in aper; possible blended EB
C7	218916923.01	11.5	0.93	S	28.4	$9.36^{+0.03}_{-0.03}$	$4.94^{+0.02}_{-0.02}$	$0.08^{+0.08}_{-0.06}$	$9.5^{+0.6}_{-0.5}$	0	

Table 1 continued

Table 1 *(continued)*

	Cand.	Kp	$R_\star$	Prov.	P	$R_P/R_\star$	T_{14}	b	R_P	EB	Comments
		mag	$R_\odot$		days	%	hr		$R_\oplus$		
C7	214611894.01	11.9	1.21	S	21.6	$15.57^{+0.13}_{-0.06}$	$4.07^{+0.02}_{-0.02}$	$0.11^{+0.10}_{-0.08}$	$20.5^{+2.8}_{-2.1}$	0	Deep ($\sim$3%); flat-bottom
C7	213546283.01	12.0	1.10	S	9.8	$2.77^{+0.24}_{-0.12}$	$2.98^{+0.15}_{-0.14}$	$0.48^{+0.31}_{-0.33}$	$3.3^{+0.6}_{-0.4}$	0	
C7	215938010.01	12.1	1.64	S	1.2	$6.91^{+5.16}_{-3.22}$	$0.00^{+0.00}_{-0.00}$	$1.28^{+0.12}_{-0.12}$	$12.4^{+9.4}_{-5.9}$	0	
C7	216494238.01	12.3	1.45	S	19.9	$5.37^{+0.14}_{-0.08}$	$8.19^{+0.12}_{-0.07}$	$0.37^{+0.19}_{-0.25}$	$8.5^{+1.2}_{-1.0}$	0	
C7	219388192.01	12.3	1.00	S	5.3	$8.79^{+0.09}_{-0.05}$	$3.30^{+0.03}_{-0.02}$	$0.16^{+0.15}_{-0.11}$	$9.6^{+0.7}_{-0.5}$	0	
C7	218621322.01	12.4	1.00	S	11.6	$20.20^{+46.42}_{-15.46}$	$3.90^{+0.73}_{-3.90}$	$1.17^{+0.51}_{-0.21}$	$21.9^{+50.5}_{-16.9}$	0	Variable depth, poss. contam. nearby source%
C7	216892056.01	12.5	0.42	P	2.8	$4.13^{+0.43}_{-0.21}$	$0.50^{+0.06}_{-0.03}$	$0.46^{+0.32}_{-0.31}$	$1.9^{+0.8}_{-0.8}$	0	
C7	217192839.01	12.6	0.70	S	16.0	$2.60^{+0.31}_{-0.15}$	$3.07^{+0.22}_{-0.20}$	$0.48^{+0.32}_{-0.32}$	$2.0^{+0.4}_{-0.3}$	0	
C7	218131080.01	12.7	1.22	S	3.1	$5.87^{+0.08}_{-0.04}$	$4.48^{+0.03}_{-0.02}$	$0.21^{+0.18}_{-0.15}$	$7.8^{+0.9}_{-0.6}$	0	HAT-S-12 b
C7	216468514.01	12.7	1.73	S	3.3	$7.64^{+0.19}_{-0.18}$	$2.98^{+0.06}_{-0.05}$	$0.50^{+0.13}_{-0.21}$	$14.4^{+2.2}_{-1.9}$	0	
C7	219420915.01	12.8	1.30	S	0.5	$18.38^{+7.76}_{-4.18}$	$0.00^{+0.00}_{-0.00}$	$1.31^{+0.11}_{-0.10}$	$26.1^{+11.6}_{-6.6}$	0	V-shaped
C7	216334329.01	12.9	1.54	S	28.1	$39.99^{+40.06}_{-26.41}$	$3.62^{+0.20}_{-0.18}$	$1.35^{+0.41}_{-0.28}$	$67.3^{+68.1}_{-45.1}$	0	
C7	219256848.01	13.1	11.57	S	20.9	$46.86^{+35.73}_{-28.86}$	$3.49^{+0.19}_{-0.18}$	$1.39^{+0.37}_{-0.31}$	$591.1^{+453.8}_{-367.2}$	0	
C7	217671466.01	13.1	1.94	S	1.9	$8.13^{+0.09}_{-0.04}$	$3.56^{+0.02}_{-0.01}$	$0.13^{+0.12}_{-0.09}$	$17.2^{+2.9}_{-2.2}$	0	Known HAT-S system
C7	215389654.01	13.2	0.97	S	23.5	$17.41^{+0.27}_{-0.11}$	$8.58^{+0.11}_{-0.12}$	$0.20^{+0.16}_{-0.14}$	$18.4^{+1.8}_{-1.2}$	0	Deep ($\sim$4%); flat-bottom
C7	213840781.01	13.7	0.76	P	12.4	$43.63^{+26.02}_{-15.25}$	$2.86^{+0.09}_{-0.12}$	$1.03^{+0.31}_{-0.23}$	$36.3^{+26.0}_{-19.3}$	0	Deep ($\sim$4%); V-shaped;
C7	216414930.01	13.7	0.89	P	3.6	$10.52^{+0.05}_{-0.03}$	$4.42^{+0.01}_{-0.01}$	$0.07^{+0.08}_{-0.05}$	$10.2^{+4.1}_{-4.1}$	0	
C7	215358983.01	13.8	1.10	S	6.4	$12.79^{+0.13}_{-0.07}$	$6.12^{+0.04}_{-0.04}$	$0.11^{+0.11}_{-0.08}$	$15.3^{+1.8}_{-1.4}$	0	Deep ($\sim$2%); flat-bottomed
C7	213703832.01	13.9	0.75	P	0.5	$4.09^{+0.96}_{-0.51}$	$1.31^{+0.11}_{-1.31}$	$0.69^{+0.46}_{-0.48}$	$3.4^{+1.6}_{-1.4}$	0	2 stars in aper; possible blended EB
C7	214741009.01	14.0	0.73	P	7.3	$41.56^{+38.08}_{-27.99}$	$2.36^{+0.14}_{-0.15}$	$1.29^{+0.40}_{-0.34}$	$32.9^{+32.9}_{-25.8}$	0	V-shaped
C7	217149884.01	14.2	0.90	P	16.7	$17.33^{+0.18}_{-0.13}$	$5.53^{+0.04}_{-0.04}$	$0.54^{+0.02}_{-0.03}$	$17.0^{+6.8}_{-6.8}$	0	Deep ($\sim$3%); flat-bottomed;
C7	215969174.01	14.3	1.15	S	4.2	$10.69^{+0.07}_{-0.04}$	$3.38^{+0.01}_{-0.01}$	$0.11^{+0.10}_{-0.07}$	$13.4^{+1.5}_{-1.1}$	0	
C7	215101303.01	14.9	0.84	P	15.2	$13.85^{+0.40}_{-0.20}$	$3.55^{+0.07}_{-0.05}$	$0.28^{+0.19}_{-0.19}$	$12.7^{+5.1}_{-5.1}$	0	Deep ($\sim$3%); flat-bottomed;
C7	213951550.01	15.0	0.27	P	1.1	$57.27^{+26.37}_{-18.47}$	$1.78^{+0.09}_{-0.08}$	$1.11^{+0.32}_{-0.27}$	$16.9^{+10.3}_{-8.7}$	0	Deep ($\sim$6%); V-shaped;
C7	217393088.01	15.3	1.54	S	1.3	$9.87^{+0.15}_{-0.08}$	$3.13^{+0.03}_{-0.03}$	$0.16^{+0.15}_{-0.11}$	$16.6^{+2.4}_{-2.0}$	0	
C8	220542353.01	8.8	1.91	S	15.2	$37.44^{+9.47}_{-5.31}$	$3.76^{+0.01}_{-0.01}$	$1.06^{+0.11}_{-0.07}$	$78.0^{+23.2}_{-15.1}$	0	Deep ($\sim$4%); V-shaped
C8	220383386.01	8.9	0.88	S	1.0	$1.83^{+0.22}_{-0.09}$	$1.65^{+0.05}_{-0.08}$	$0.49^{+0.33}_{-0.33}$	$1.8^{+0.2}_{-0.1}$	0	Multi; HD3167b; Vanderburg+16
C8	220383386.02	8.9	0.88	S	29.8	$3.12^{+0.51}_{-0.24}$	$5.06^{+0.49}_{-0.17}$	$0.63^{+0.27}_{-0.42}$	$3.0^{+0.5}_{-0.3}$	0	Multi; HD3167c; Vanderburg+16
C8	220666988.01	9.3	1.03	P	0.9	$37.34^{+28.78}_{-21.21}$	$0.00^{+1.11}_{-0.00}$	$1.50^{+0.45}_{-0.38}$	$42.0^{+36.5}_{-29.2}$	1	
C8	220709978.01	9.4	0.96	S	15.4	$2.02^{+0.22}_{-0.10}$	$4.39^{+0.17}_{-0.16}$	$0.47^{+0.30}_{-0.32}$	$2.1^{+0.3}_{-0.2}$	0	
C8	220303276.01	10.9	1.38	S	4.0	$8.03^{+0.01}_{-0.01}$	$4.93^{+0.01}_{-0.01}$	$0.04^{+0.04}_{-0.03}$	$12.0^{+1.2}_{-0.9}$	0	WASP-118b
C8	220725183.01	11.5	1.58	S	2.3	$30.02^{+0.72}_{-0.60}$	$4.03^{+0.00}_{-0.00}$	$0.88^{+0.01}_{-0.01}$	$51.6^{+7.6}_{-6.2}$	0	Deep ($\sim$5%); V-shape
C8	220376054.01	11.6	1.29	S	8.6	$1.75^{+0.22}_{-0.09}$	$3.73^{+0.14}_{-0.12}$	$0.48^{+0.31}_{-0.33}$	$2.5^{+0.5}_{-0.3}$	0	
C8	220621788.01	11.8	0.99	S	13.7	$2.13^{+0.25}_{-0.11}$	$3.12^{+0.11}_{-0.10}$	$0.47^{+0.30}_{-0.32}$	$2.3^{+0.4}_{-0.2}$	0	
C8	220674823.01	12.0	0.97	S	0.6	$1.74^{+0.19}_{-0.08}$	$1.45^{+0.07}_{-0.16}$	$0.48^{+0.38}_{-0.33}$	$1.8^{+0.3}_{-0.1}$	0	Multi
C8	220674823.02	12.0	0.97	S	13.3	$2.65^{+0.36}_{-0.15}$	$3.44^{+0.18}_{-0.16}$	$0.47^{+0.32}_{-0.32}$	$2.8^{+0.5}_{-0.2}$	0	Multi
C8	220481411.01	12.1	0.71	S	2.2	$2.22^{+0.29}_{-0.12}$	$1.83^{+0.05}_{-0.05}$	$0.49^{+0.31}_{-0.33}$	$1.7^{+0.3}_{-0.3}$	0	
C8	220294712.01	12.3	1.09	S	23.6	$2.51^{+0.24}_{-0.10}$	$5.84^{+0.20}_{-0.17}$	$0.46^{+0.29}_{-0.31}$	$3.0^{+0.4}_{-0.3}$	0	
C8	220555384.01	12.4	0.55	P	4.3	$2.01^{+0.34}_{-0.15}$	$1.17^{+0.08}_{-0.08}$	$0.50^{+0.31}_{-0.34}$	$1.2^{+0.5}_{-0.5}$	0	V-shaped
C8	220321605.01	12.6	0.67	S	9.8	$3.57^{+0.40}_{-0.18}$	$2.60^{+0.07}_{-0.05}$	$0.45^{+0.26}_{-0.29}$	$2.6^{+0.5}_{-0.4}$	0	
C8	220397060.01	12.8	0.84	S	12.1	$5.10^{+0.29}_{-0.11}$	$8.51^{+0.11}_{-0.08}$	$0.28^{+0.22}_{-0.19}$	$4.7^{+5.1}_{-0.4}$	0	
C8	220187552.01	12.8	0.66	S	17.1	$45.14^{+28.57}_{-18.70}$	$2.26^{+0.02}_{-0.02}$	$1.20^{+0.31}_{-0.23}$	$32.5^{+21.2}_{-14.3}$	0	Deep ($\sim$2%); V-shaped
C8	220431824.01	13.0	1.45	S	9.1	$11.55^{+0.04}_{-0.02}$	$6.91^{+0.02}_{-0.01}$	$0.07^{+0.07}_{-0.05}$	$18.3^{+2.4}_{-3.1}$	1	
C8	220621087.01	13.4	0.45	S	3.8	$2.99^{+0.53}_{-0.24}$	$1.54^{+0.11}_{-0.10}$	$0.52^{+0.29}_{-0.35}$	$1.5^{+0.4}_{-0.3}$	0	
C8	220504338.01	13.5	1.33	S	5.8	$8.65^{+0.21}_{-0.25}$	$2.89^{+0.06}_{-0.06}$	$0.58^{+0.08}_{-0.15}$	$12.5^{+1.7}_{-1.6}$	0	
C8	220501947.01	13.5	0.73	S	4.0	$12.94^{+0.04}_{-0.02}$	$2.48^{+0.01}_{-0.00}$	$0.06^{+0.06}_{-0.04}$	$10.3^{+1.4}_{-1.4}$	0	Deep ($\sim$2%); V-shape

Table 1 *(continued)*

	Cand.	Kp	$R_\star$	Prov.	P	$R_P/R_\star$	T_{14}	b	R_P	EB	Comments
		mag	$R_\odot$		days	%	hr		$R_\oplus$		
C8	220258394.01	13.7	0.87	S	16.0	$20.49^{+0.13}_{-0.10}$	$4.89^{+0.02}_{-0.02}$	$0.70^{+0.01}_{-0.01}$	$19.5^{+0.9}_{-0.8}$	0	Deep ($\sim$5%); V-shape
C8	220554210.01	13.7	0.93	S	4.2	$2.70^{+0.34}_{-0.14}$	$2.73^{+0.11}_{-0.11}$	$0.48^{+0.31}_{-0.32}$	$2.7^{+0.4}_{-0.2}$	0	
C8	220436208.01	13.9	1.17	S	5.2	$3.37^{+0.34}_{-0.13}$	$3.45^{+0.10}_{-0.09}$	$0.44^{+0.30}_{-0.30}$	$4.3^{+0.7}_{-0.5}$	0	
C8	220629489.01	14.1	0.86	S	1.9	$4.04^{+0.48}_{-0.18}$	$1.75^{+0.06}_{-0.04}$	$0.45^{+0.32}_{-0.31}$	$3.8^{+0.5}_{-0.2}$	0	
C8	220565349.01	14.1	0.84	S	21.8	$21.77^{+23.83}_{-6.56}$	$2.20^{+0.05}_{-0.21}$	$0.91^{+0.31}_{-0.23}$	$19.9^{+21.8}_{-6.0}$	0	Deep ($\sim$2%); V-shape
C8	220209578.01	14.4	0.89	S	8.9	$38.05^{+32.87}_{-20.38}$	$2.95^{+0.06}_{-0.07}$	$1.24^{+0.35}_{-0.25}$	$36.9^{+32.0}_{-19.9}$	0	V-shaped
C8	220522262.01	14.8	0.75	S	8.7	$9.89^{+0.33}_{-0.14}$	$2.75^{+0.04}_{-0.03}$	$0.23^{+0.21}_{-0.16}$	$8.1^{+1.1}_{-1.1}$	0	
C8	220696233.01	15.5	0.35	P	28.7	$10.49^{+0.88}_{-0.38}$	$2.99^{+0.26}_{-0.11}$	$0.36^{+0.26}_{-0.25}$	$4.0^{+1.6}_{-1.6}$	0	
C8	220336320.01	15.9	0.37	P	1.7	$52.53^{+25.35}_{-21.65}$	$1.37^{+0.02}_{-0.02}$	$1.17^{+0.29}_{-0.29}$	$21.3^{+13.3}_{-12.2}$	0	Deep ($\sim$5%); V-shaped
C8	220448185.01	16.0	0.69	P	0.7	$22.87^{+42.13}_{-3.88}$	$0.37^{+0.07}_{-0.06}$	$0.67^{+0.66}_{-0.49}$	$17.2^{+32.5}_{-7.5}$	0	Half the reported period

NOTE—*K2* objects of interest (K2OIs) identified through our systematic search of *K2* photometry sorted by campaign and *Kepler* magnitude (Kp). For each candidate we quote the highest quality stellar radius ($R_\star$) computed from spectroscopy (S), where available, and from photometry (P), otherwise. Planet orbital period (P), planet-to-star radius ratio ($R_P/R_\star$), time between first and last contact (T_{14}), and impact parameter (b) are provided. The full precision and uncertainties on P and time of first transit T_0 are provided in the machine-readable version of this table. R_P is the derived planetary radius given the light curve fit and stellar radius. We also include a summary of our eclipsing binary assessment: 'EB' is a numerical code designating whether or the object of interest was a likely EB: 0—no obvious indication of EB, 1—secondary eclipse visible, 2—photometric variability that is phase-locked to the eclipse. Some additional comments on individual systems are provided.

Table 2. Stars with HIRES Spectra and Derived Parameters

Camp.	EPIC	Kp	$T_{\rm eff}$	$\log g$	[Fe/H]	$v \sin i$	$M_\star$	$R_\star$	SM[a]	SB2[b]	disp[c]
		mag	K	cgs	dex	km s^{-1}	$M_\odot$	$R_\odot$			
C5	211401787	9.7	6214	4.26	-0.04	8.4	$1.12^{+0.06}_{-0.05}$	$1.25^{+0.17}_{-0.12}$	1	1	PC
C5	211945201	10.1	6018	4.13	0.12	3.3	$1.17^{+0.10}_{-0.08}$	$1.48^{+0.21}_{-0.19}$	1	1	PC
C5	211990866	10.4	6180	4.51	0.32	13.6	$1.25^{+0.05}_{-0.04}$	$1.23^{+0.09}_{-0.06}$	1	1	PC
C5	212099230	10.5	5487	4.41	0.11	1.6	$0.93^{+0.04}_{-0.04}$	$0.96^{+0.09}_{-0.06}$	1	1	PC
C5	211594205	10.7	5240	4.69	-0.05	1.5	$0.83^{+0.03}_{-0.03}$	$0.79^{+0.04}_{-0.03}$	1	1	PC
C5	212110888	11.4	6008	4.16	0.01	5.9	$1.09^{+0.09}_{-0.06}$	$1.38^{+0.19}_{-0.17}$	1	4	PC
C5	211525389	11.7	5479	4.48	0.30	2.4	$1.00^{+0.04}_{-0.04}$	$0.98^{+0.08}_{-0.05}$	1	1	PC
C5	211359660	11.7	5177	4.62	0.12	2.0	$0.87^{+0.03}_{-0.03}$	$0.82^{+0.04}_{-0.03}$	1	1	PC
C5	212012119	11.8	4929	4.73	0.05	4.7	$0.80^{+0.03}_{-0.03}$	$0.75^{+0.03}_{-0.02}$	1	1	PC
C5	211491383	11.8	6141	4.21	-0.13	6.1	$1.06^{+0.06}_{-0.05}$	$1.28^{+0.18}_{-0.15}$	1	1	PC
C5	211391664	12.1	6074	4.12	-0.11	6.7	$1.05^{+0.08}_{-0.06}$	$1.39^{+0.19}_{-0.17}$	1	1	PC
C5	211736671	12.2	5554	3.93	0.40	2.6	$1.18^{+0.10}_{-0.09}$	$1.77^{+0.27}_{-0.23}$	1	1	PC
C5	211319617	12.4	5156	4.72	-0.60	0.8	$0.69^{+0.03}_{-0.03}$	$0.65^{+0.02}_{-0.02}$	1	1	PC
C5	211342524	12.4	6168	4.14	-0.19	7.8	$1.04^{+0.07}_{-0.06}$	$1.36^{+0.19}_{-0.16}$	1	5	PC
C5	211351816	12.4	4803	3.19	0.40	3.7	$1.45^{+0.25}_{-0.22}$	$4.79^{+0.86}_{-0.67}$	1	1	PC
C5	211800191	12.4	5919	4.53	-0.51	1.3	$0.85^{+0.04}_{-0.04}$	$0.84^{+0.06}_{-0.04}$	1	1	PC
C5	212006344	12.5	3925	$\cdots$	0.43	$\cdots$	$\cdots$	$0.63^{+0.10}_{-0.10}$	2	1	PC
C5	211355342	12.6	5606	4.32	0.27	1.9	$1.03^{+0.05}_{-0.05}$	$1.11^{+0.14}_{-0.10}$	1	1	PC
C5	212164470	12.7	5893	4.24	-0.04	2.8	$1.00^{+0.05}_{-0.05}$	$1.19^{+0.16}_{-0.13}$	1	1	PC
C5	211562654	12.8	5442	4.43	0.09	1.2	$0.91^{+0.04}_{-0.04}$	$0.92^{+0.08}_{-0.06}$	1	1	PC
C5	212008766	12.8	5038	4.68	-0.12	1.7	$0.77^{+0.03}_{-0.03}$	$0.74^{+0.03}_{-0.03}$	1	1	PC
C5	212157262	12.9	5459	4.48	0.25	1.6	$0.97^{+0.04}_{-0.04}$	$0.96^{+0.07}_{-0.05}$	1	1	PC
C5	212138198	12.9	5138	4.40	0.29	1.9	$0.90^{+0.03}_{-0.03}$	$0.89^{+0.06}_{-0.05}$	1	1	PC
C5	211818569	12.9	4526	$\cdots$	0.04	$\cdots$	$\cdots$	$0.71^{+0.10}_{-0.10}$	2	1	PC
C5	211439059	13.1	5481	4.72	-0.01	4.3	$0.90^{+0.03}_{-0.04}$	$0.84^{+0.04}_{-0.03}$	1	4	PC

Table 2 *(continued)*

Camp.	EPIC	Kp	$T_{\rm eff}$	$\log g$	[Fe/H]	$v \sin i$	$M_\star$	$R_\star$	SM[a]	SB2[b]	disp[c]
		mag	K	cgs	dex	km s^{-1}	$M_\odot$	$R_\odot$			
C5	211919004	13.1	5149	4.51	0.22	1.4	$0.89^{+0.04}_{-0.03}$	$0.86^{+0.05}_{-0.04}$	1	1	PC
C5	211442297	13.2	5596	4.55	-0.12	0.9	$0.89^{+0.04}_{-0.04}$	$0.86^{+0.06}_{-0.04}$	1	1	PC
C5	211490999	13.4	5488	4.42	-0.02	0.9	$0.89^{+0.04}_{-0.04}$	$0.91^{+0.07}_{-0.06}$	1	1	PC
C5	211529065	13.4	4915	4.53	0.31	3.5	$0.86^{+0.03}_{-0.03}$	$0.82^{+0.03}_{-0.03}$	1	1	PC
C5	211413752	13.5	5025	4.61	0.04	1.5	$0.81^{+0.03}_{-0.03}$	$0.78^{+0.03}_{-0.03}$	1	1	PC
C5	211713099	13.6	5532	4.37	-0.35	0.6	$0.80^{+0.03}_{-0.03}$	$0.83^{+0.06}_{-0.05}$	1	1	PC
C5	211816003	13.7	5313	4.61	-0.34	0.3	$0.77^{+0.03}_{-0.03}$	$0.74^{+0.03}_{-0.03}$	1	1	PC
C5	211331236	13.9	3687	$\cdots$	-0.17	$\cdots$	$\cdots$	$0.52^{+0.10}_{-0.10}$	2	1	PC
C5	212069861	14.1	3926	$\cdots$	0.18	$\cdots$	$\cdots$	$0.64^{+0.10}_{-0.10}$	2	1	PC
C5	211929937	14.2	5230	4.54	0.10	0.6	$0.87^{+0.03}_{-0.03}$	$0.84^{+0.04}_{-0.04}$	1	1	PC
C5	211418729	14.3	5020	4.33	0.45	2.7	$0.90^{+0.03}_{-0.03}$	$0.90^{+0.06}_{-0.05}$	1	1	PC
C5	211578235	14.3	5491	4.25	-0.16	4.1	$0.85^{+0.04}_{-0.03}$	$0.94^{+0.14}_{-0.08}$	1	5	PC
C5	211399359	14.4	4972	4.64	0.04	3.2	$0.80^{+0.03}_{-0.03}$	$0.77^{+0.03}_{-0.03}$	1	1	PC
C5	211978865	14.4	6519	4.33	-0.19	18.7	$1.15^{+0.05}_{-0.05}$	$1.21^{+0.13}_{-0.08}$	1	3	PC
C5	212130773	14.5	4949	4.55	0.04	1.8	$0.80^{+0.03}_{-0.03}$	$0.77^{+0.03}_{-0.03}$	1	1	PC
C5	211770795	14.5	4454	$\cdots$	0.08	$\cdots$	$\cdots$	$0.71^{+0.10}_{-0.10}$	2	1	PC
C5	212154564	15.1	$\cdots$	$\cdots$	$\cdots$	65.7	$\cdots$	$\cdots$	0	1	PC
C5	211916756	15.5	$\cdots$	$\cdots$	$\cdots$	252.7	$\cdots$	$\cdots$	0	1	PC
C6	212357477	10.2	5741	4.46	0.12	2.4	$1.02^{+0.05}_{-0.05}$	$1.01^{+0.08}_{-0.06}$	1	1	PC
C6	212703473	10.7	5816	4.38	0.19	5.2	$1.08^{+0.05}_{-0.05}$	$1.11^{+0.12}_{-0.08}$	1	3	PC
C6	212803289	11.0	6102	3.96	0.20	10.0	$1.40^{+0.13}_{-0.12}$	$1.98^{+0.31}_{-0.27}$	1	1	PC
C6	212782836	11.6	5418	4.48	-0.42	1.1	$0.76^{+0.03}_{-0.03}$	$0.76^{+0.04}_{-0.03}$	1	1	PC
C6	212521166	11.6	4895	4.64	-0.24	1.9	$0.71^{+0.03}_{-0.03}$	$0.68^{+0.02}_{-0.02}$	1	1	PC
C6	212586030	11.7	4865	3.37	0.38	3.5	$1.41^{+0.21}_{-0.19}$	$3.83^{+0.62}_{-0.52}$	1	1	PC
C6	212300977	11.7	5965	4.34	0.00	2.7	$1.04^{+0.05}_{-0.05}$	$1.11^{+0.13}_{-0.09}$	1	1	PC
C6	212779596	11.9	4507	$\cdots$	-0.04	$\cdots$	$\cdots$	$0.70^{+0.10}_{-0.10}$	2	1	PC
C6	212735333	12.0	5660	4.50	0.09	1.3	$0.98^{+0.04}_{-0.05}$	$0.96^{+0.07}_{-0.05}$	1	1	PC
C6	212587672	12.2	5948	4.49	-0.21	2.1	$0.95^{+0.04}_{-0.04}$	$0.95^{+0.08}_{-0.05}$	1	1	PC
C6	212697709	12.2	5719	4.28	0.28	1.6	$1.09^{+0.06}_{-0.05}$	$1.20^{+0.17}_{-0.13}$	1	1	PC
C6	212394689	12.2	5456	4.50	-0.01	1.6	$0.89^{+0.04}_{-0.04}$	$0.88^{+0.06}_{-0.04}$	1	1	PC
C6	212689874	12.3	5644	4.36	-0.12	1.7	$0.88^{+0.04}_{-0.04}$	$0.95^{+0.10}_{-0.07}$	1	1	PC
C6	212435047	12.4	5750	4.29	0.01	2.0	$0.96^{+0.05}_{-0.05}$	$1.10^{+0.14}_{-0.11}$	1	1	PC
C6	212460519	12.4	4226	$\cdots$	-0.17	$\cdots$	$\cdots$	$0.66^{+0.10}_{-0.10}$	2	1	PC
C6	212428509	12.5	5697	4.25	-0.42	1.7	$0.81^{+0.03}_{-0.03}$	$0.94^{+0.15}_{-0.08}$	1	1	PC
C6	212585579	12.6	5931	4.35	-0.00	2.3	$1.02^{+0.05}_{-0.05}$	$1.09^{+0.12}_{-0.09}$	1	1	PC
C7	213920015	10.0	5682	4.60	-0.12	2.1	$0.91^{+0.04}_{-0.04}$	$0.87^{+0.05}_{-0.04}$	1	1	PC
C7	218711655	11.3	6404	4.18	0.08	6.9	$1.29^{+0.08}_{-0.06}$	$1.46^{+0.22}_{-0.16}$	1	1	PC
C7	218916923	11.5	5393	4.57	0.29	1.7	$0.97^{+0.04}_{-0.04}$	$0.93^{+0.06}_{-0.04}$	1	1	PC
C7	214611894	11.9	6072	4.27	-0.02	4.8	$1.07^{+0.06}_{-0.05}$	$1.21^{+0.17}_{-0.12}$	1	1	PC
C7	213546283	12.0	5685	4.23	-0.14	0.1	$0.89^{+0.04}_{-0.03}$	$1.10^{+0.17}_{-0.12}$	1	1	PC
C7	215938010	12.1	6027	4.03	0.08	3.5	$1.20^{+0.11}_{-0.09}$	$1.64^{+0.24}_{-0.20}$	1	1	PC
C7	216494238	12.3	5741	4.14	0.35	2.5	$1.17^{+0.10}_{-0.08}$	$1.45^{+0.20}_{-0.18}$	1	1	PC
C7	219388192	12.3	5781	4.54	0.12	4.2	$1.03^{+0.05}_{-0.04}$	$1.00^{+0.07}_{-0.05}$	1	1	PC
C7	218621322	12.4	5675	4.26	-0.27	0.3	$0.85^{+0.03}_{-0.03}$	$1.00^{+0.16}_{-0.10}$	1	1	PC
C7	216892056	12.5	$\cdots$	$\cdots$	$\cdots$	64.1	$\cdots$	$\cdots$	0	1	PC
C7	217192839	12.6	4541	$\cdots$	-0.28	$\cdots$	$\cdots$	$0.70^{+0.10}_{-0.10}$	2	1	PC
C7	218131080	12.7	6394	4.32	-0.09	4.5	$1.15^{+0.05}_{-0.05}$	$1.22^{+0.14}_{-0.09}$	1	1	PC
C7	216468514	12.7	6038	4.02	0.16	4.7	$1.28^{+0.12}_{-0.11}$	$1.73^{+0.26}_{-0.23}$	1	1	PC
C7	219420915	12.8	5815	4.24	0.32	2.9	$1.15^{+0.08}_{-0.06}$	$1.30^{+0.18}_{-0.14}$	1	1	PC

Table 2 continued

Table 2 *(continued)*

Camp.	EPIC	Kp	$T_{\rm eff}$	$\log g$	[Fe/H]	$v \sin i$	$M_\star$	$R_\star$	SM[a]	SB2[b]	disp[c]
		mag	K	cgs	dex	km s^{-1}	$M_\odot$	$R_\odot$			
C7	216334329	12.9	5830	4.05	0.13	2.3	$1.12^{+0.10}_{-0.07}$	$1.54^{+0.23}_{-0.18}$	1	1	PC
C7	219256848	13.1	4530	2.57	0.32	4.2	$1.76^{+0.44}_{-0.35}$	$11.57^{+1.03}_{-0.94}$	1	1	PC
C7	217671466	13.1	5576	3.87	0.43	3.7	$1.25^{+0.12}_{-0.10}$	$1.94^{+0.33}_{-0.25}$	1	1	PC
C7	215389654	13.2	5416	4.41	0.24	1.2	$0.96^{+0.04}_{-0.04}$	$0.97^{+0.09}_{-0.06}$	1	1	PC
C7	213840781	13.7	$\cdots$	$\cdots$	$\cdots$	137.1	$\cdots$	$\cdots$	0	5	PC
C7	215358983	13.8	6135	4.31	-0.24	11.2	$0.99^{+0.05}_{-0.05}$	$1.10^{+0.13}_{-0.10}$	1	1	PC
C7	215969174	14.3	5929	4.35	0.16	3.8	$1.11^{+0.05}_{-0.05}$	$1.15^{+0.13}_{-0.09}$	1	1	PC
C7	217393088	15.3	5839	4.09	0.25	5.1	$1.19^{+0.11}_{-0.08}$	$1.54^{+0.22}_{-0.19}$	1	1	PC
C8	220542353	8.8	6414	3.86	-0.45	8.5	$1.12^{+0.09}_{-0.07}$	$1.91^{+0.30}_{-0.25}$	1	5	PC
C8	220383386	8.9	5305	4.47	0.11	0.0	$0.89^{+0.04}_{-0.03}$	$0.88^{+0.06}_{-0.04}$	1	1	PC
C8	220709978	9.4	5963	4.44	-0.25	2.6	$0.93^{+0.04}_{-0.04}$	$0.96^{+0.09}_{-0.06}$	1	1	PC
C8	220303276	10.9	6446	4.29	0.15	10.7	$1.31^{+0.06}_{-0.05}$	$1.38^{+0.14}_{-0.10}$	1	3	PC
C8	220725183	11.5	6188	4.05	-0.07	18.8	$1.16^{+0.10}_{-0.08}$	$1.58^{+0.23}_{-0.19}$	1	5	PC
C8	220376054	11.6	5863	4.19	0.06	2.5	$1.05^{+0.07}_{-0.06}$	$1.29^{+0.18}_{-0.15}$	1	1	PC
C8	220621788	11.8	5652	4.40	0.05	0.9	$0.95^{+0.05}_{-0.04}$	$0.99^{+0.10}_{-0.07}$	1	1	PC
C8	220674823	12.0	5547	4.44	0.14	1.4	$0.96^{+0.05}_{-0.04}$	$0.97^{+0.09}_{-0.06}$	1	1	PC
C8	220481411	12.1	4495	$\cdots$	0.08	$\cdots$	$\cdots$	$0.71^{+0.10}_{-0.10}$	2	1	PC
C8	220294712	12.3	6100	4.36	-0.11	4.3	$1.04^{+0.05}_{-0.05}$	$1.09^{+0.12}_{-0.08}$	1	1	PC
C8	220321605	12.6	4159	$\cdots$	-0.01	$\cdots$	$\cdots$	$0.67^{+0.10}_{-0.10}$	2	1	PC
C8	220397060	12.8	5221	4.16	-0.21	3.6	$0.81^{+0.11}_{-0.04}$	$0.84^{+0.91}_{-0.07}$	1	5	PC
C8	220187552	12.8	4197	$\cdots$	-0.02	$\cdots$	$\cdots$	$0.66^{+0.10}_{-0.10}$	2	4	PC
C8	220621087	13.4	3633	$\cdots$	-0.28	$\cdots$	$\cdots$	$0.45^{+0.10}_{-0.10}$	2	1	PC
C8	220504338	13.5	5648	4.18	0.30	2.0	$1.08^{+0.08}_{-0.06}$	$1.33^{+0.18}_{-0.16}$	1	1	PC
C8	220501947	13.5	4398	$\cdots$	0.17	$\cdots$	$\cdots$	$0.73^{+0.10}_{-0.10}$	2	1	PC
C8	220258394	13.7	5601	4.81	0.03	3.9	$0.94^{+0.04}_{-0.03}$	$0.87^{+0.04}_{-0.04}$	1	5	PC
C8	220554210	13.7	5440	4.47	0.16	1.2	$0.94^{+0.04}_{-0.04}$	$0.93^{+0.07}_{-0.05}$	1	1	PC
C8	220436208	13.9	5645	4.29	0.28	2.3	$1.05^{+0.06}_{-0.05}$	$1.17^{+0.16}_{-0.12}$	1	1	PC
C8	220629489	14.1	5050	4.47	0.32	2.7	$0.88^{+0.04}_{-0.03}$	$0.86^{+0.05}_{-0.03}$	1	1	PC
C8	220565349	14.1	5453	4.61	-0.06	3.2	$0.87^{+0.04}_{-0.04}$	$0.84^{+0.05}_{-0.03}$	1	1	PC
C8	220209578	14.4	5757	4.47	-0.26	3.8	$0.87^{+0.04}_{-0.04}$	$0.89^{+0.07}_{-0.05}$	1	1	PC
C8	220522262	14.8	4616	$\cdots$	0.15	$\cdots$	$\cdots$	$0.75^{+0.10}_{-0.10}$	2	1	PC
C6	212727070	9.4	$\cdots$	$\cdots$	$\cdots$	20.1	$\cdots$	$\cdots$	0	3	EB
C6	212351868	10.2	$\cdots$	$\cdots$	$\cdots$	46.0	$\cdots$	$\cdots$	0	3	EB
C6	212773309	11.4	5009	4.42	0.36	9.1	$0.88^{+0.03}_{-0.03}$	$0.86^{+0.05}_{-0.04}$	1	1	EB
C7	218541396	10.0	$\cdots$	$\cdots$	$\cdots$	21.2	$\cdots$	$\cdots$	0	3	EB
C8	220666988	9.3	$\cdots$	$\cdots$	$\cdots$	32.6	$\cdots$	$\cdots$	0	1	EB
C8	220431824	13.0	5434	4.10	0.04	8.6	$0.95^{+0.05}_{-0.03}$	$1.45^{+0.19}_{-0.24}$	1	1	EB
C5	212066407	12.2	5857	4.31	-0.12	2.4	$0.94^{+0.05}_{-0.05}$	$1.07^{+0.13}_{-0.10}$	1	1	EB
C6	212651120	10.5	$\cdots$	$\cdots$	$\cdots$	128.0	$\cdots$	$\cdots$	0	3	EB
C5	211993818	7.2	5228	3.06	-0.08	6.1	$2.09^{+0.21}_{-0.26}$	$8.03^{+1.18}_{-2.32}$	1	5	Other
C5	211311380	9.1	6251	4.28	0.00	5.7	$1.15^{+0.06}_{-0.05}$	$1.25^{+0.16}_{-0.11}$	1	1	Other
C5	211886472	11.1	6458	4.32	-0.04	8.0	$1.20^{+0.05}_{-0.05}$	$1.26^{+0.13}_{-0.08}$	1	1	Other
C5	211987231	11.7	6103	4.44	-0.04	5.5	$1.07^{+0.05}_{-0.05}$	$1.08^{+0.09}_{-0.07}$	1	4	Other
C5	211941472	11.8	5767	4.06	-0.00	2.6	$1.01^{+0.07}_{-0.06}$	$1.45^{+0.22}_{-0.18}$	1	1	Other
C5	211770696	12.3	5786	4.22	-0.31	1.5	$0.86^{+0.04}_{-0.03}$	$1.09^{+0.18}_{-0.13}$	1	1	Other
C5	211645912	12.5	5899	4.60	0.01	4.2	$1.02^{+0.04}_{-0.04}$	$0.98^{+0.06}_{-0.05}$	1	1	Other
C5	211743874	12.5	6182	4.32	0.12	6.0	$1.18^{+0.05}_{-0.05}$	$1.24^{+0.13}_{-0.10}$	1	1	Other
C5	212006318	12.9	5822	4.11	0.03	2.1	$1.03^{+0.07}_{-0.06}$	$1.39^{+0.20}_{-0.17}$	1	1	Other
C5	211978909	13.2	5112	3.70	-0.33	1.9	$0.96^{+0.14}_{-0.07}$	$2.41^{+0.39}_{-0.28}$	1	1	Other

Table 2 continued

Table 2 *(continued)*

Camp.	EPIC	Kp	T_{eff}	$\log g$	[Fe/H]	$v \sin i$	$M_\star$	$R_\star$	SM[a]	SB2[b]	disp[c]
		mag	K	cgs	dex	km s^{-1}	$M_\odot$	$R_\odot$			
C5	211825866	13.8	5279	4.74	-0.19	0.9	$0.80^{+0.03}_{-0.03}$	$0.76^{+0.03}_{-0.02}$	1	1	Other
C6	212473154	9.0	4740	2.68	0.01	4.3	$1.85^{+0.50}_{-0.37}$	$10.92^{+0.90}_{-1.74}$	1	1	Other
C6	212768333	11.0	5242	4.70	0.05	5.8	$0.86^{+0.03}_{-0.03}$	$0.81^{+0.04}_{-0.03}$	1	1	Other
C6	212705192	11.7	$\cdots$	$\cdots$	$\cdots$	20.8	$\cdots$	$\cdots$	0	5	Other
C6	212658818	12.1	5464	4.37	0.36	2.1	$1.01^{+0.04}_{-0.04}$	$1.05^{+0.12}_{-0.08}$	1	1	Other
C6	212393193	12.1	6252	4.51	0.01	9.3	$1.14^{+0.04}_{-0.05}$	$1.12^{+0.08}_{-0.06}$	1	1	Other
C7	214889247	9.7	5891	4.50	0.18	3.4	$1.09^{+0.05}_{-0.05}$	$1.07^{+0.08}_{-0.06}$	1	1	Other
C7	218155470	9.8	7030	2.12	-1.54	18.5	$\cdots$	$\cdots$	1	2	Other
C7	213743957	11.4	$\cdots$	$\cdots$	$\cdots$	62.5	$\cdots$	$\cdots$	0	3	Other
C7	215346008	11.8	4378	2.36	-0.02	5.1	$1.23^{+0.47}_{-0.23}$	$12.34^{+2.96}_{-1.61}$	1	1	Other
C7	216050437	12.3	$\cdots$	$\cdots$	$\cdots$	38.5	$\cdots$	$\cdots$	0	5	Other
C7	218212249	13.1	4379	2.25	-0.54	5.1	$1.01^{+0.33}_{-0.13}$	$13.91^{+2.79}_{-1.91}$	1	1	Other
C8	220503133	6.5	4776	2.68	0.03	4.5	$1.97^{+0.58}_{-0.32}$	$10.99^{+1.25}_{-1.47}$	1	1	Other
C8	220492184	8.0	6694	3.34	-0.81	15.3	$1.64^{+0.15}_{-0.12}$	$4.12^{+0.73}_{-0.57}$	1	5	Other
C8	220493203	9.9	5054	2.92	-0.46	3.9	$1.70^{+0.39}_{-0.56}$	$7.88^{+1.21}_{-2.21}$	1	1	Other
C8	220643470	10.8	4432	2.34	-0.69	4.2	$0.96^{+0.24}_{-0.11}$	$12.19^{+2.16}_{-1.39}$	1	1	Other
C8	220487418	12.1	6029	4.24	0.05	4.5	$1.10^{+0.07}_{-0.06}$	$1.27^{+0.19}_{-0.14}$	1	1	Other
C8	220209709	12.2	5911	4.14	0.02	1.6	$1.06^{+0.08}_{-0.06}$	$1.37^{+0.19}_{-0.17}$	1	1	Other
C8	220650439	12.2	5676	4.38	0.13	1.3	$0.99^{+0.05}_{-0.05}$	$1.04^{+0.11}_{-0.08}$	1	1	Other
C8	220204960	12.7	$\cdots$	$\cdots$	$\cdots$	97.6	$\cdots$	$\cdots$	0	4	Other

NOTE—The 143 stars observed by Keck/HIRES, their stellar parameters, and SB2 status (if available). We derived stellar properties using two complimentary techniques: SpecMatch-Syn (Petigura 2015) and SpecMatch-Emp (Yee et al. 2017). For stars cooler than 4700 K, we used SpecMatch-Syn to compute T_{eff}, $\log g$, and [Fe/H], which were converted into $R_\star$ and $M_\star$ using the isochrones package (Morton 2015). For stars cooler than 4700 K, we used SpecMatch-Emp to compute T_{eff}, $R_\star$, $M_\star$, and [Fe/H]. We also searched for SB2s using the methodology of Kolbl et al. (2015).

[a] Source of spectroscopic properties: 0—Spectroscopic properties are not reliable (13 stars). 1—Parameters from SpecMatch-Syn (116 stars). 2—Parameters from SpecMatch-Emp (14 stars). The spectroscopic parameters are not reliable if $T_{\mathrm{eff}} > 6500$ K or $v \sin i > 20$ km s^{-1}. SpecMatch-Syn achieves precisions of 60 K, 0.10 dex, 0.04 dex, and 1 km s^{-1} in T_{eff}, $\log g$, [Fe/H], and $v \sin i$. SpecMatch-Emp achieves precisions of 70 K in T_{eff}, 10% in $R_\star$, and 0.12 dex in [Fe/H].

[b] ReaMatch classification codes: 1—No detection, 2—Star is unfit for ReaMatch: Teff below 3500 K or above 6500K, 3—Star is unfit for ReaMatch: $v \sin i$ above 10 km s^{-1}; 4—Ambiguous detection; 5—Obvious detection.

[c] Flag indicating whether the target is a planet candidate (PC), eclipsing binary (EB), or is not included in our candidate list (Other).